

Supplementary Information for

**A smart photosensitizer based on a red emitting solution processable porous polymer:
generation of reactive oxygen species**

Sujoy Bandyopadhyay, Subhankar Kundu, Arkaprabha Giri and Abhijit Patra*

Department of Chemistry, Indian Institute of Science Education and Research Bhopal (IISERB),

Bhopal-462066, Fax: +91 (0)755 409 2392; Tel: +91 (0)755 669 1337

E-mail: abhijit@iiserb.ac.in

Sr. No.	Contents	Page No.
I.	Instrumentation	S2-S3
II.	Design strategy	S4
III.	Synthesis and characterization	S5-S15
a	Chemicals	S5
b	Synthesis and characterization of monomers	S5-S8
c	Fabrication of the soluble porous polymer (CzBDP)	S8-S9
d	Fabrication of the soluble linear polymer (CzBDP-L)	S9-S10
e	Characterization of CzBDP	S10-S12
f	Characterization of CzBDP-L	S12-S13
g	Microscopic characterizations (FESEM, HRTEM)	S14-S15
IV.	Gas sorption	S16
V.	Spectroscopic investigation	S17-S19
VI.	Cyclic voltammetry analysis	S19
VII.	Generation of reactive oxygen species	S20-S27
a	Mechanistic overview on reactive oxygen species generation	S20-S21
b	Generation of singlet oxygen	S22-S25
c	Generation of superoxide anion radical	S26-S27
VIII.	Photooxidation of benzylamine	S28-S31
IX.	Thin film fabrication and future scope	S32
X.	Comparative account of physicochemical properties of CzBDP with other notable porous materials	S33-S38
XI.	¹ H and ¹³ C NMR of all compounds	S39-S48
XII.	References	S49-S51

I. Instrumentation

Nuclear magnetic resonance (NMR) spectroscopy:

^1H NMR and ^{13}C NMR spectra were recorded on Bruker Avance III 500 and 400 MHz NMR spectrometers. The residual solvent signal was used as internal standard and chemical shifts (δ) were reported in parts per million (ppm). All NMR measurements were carried out in CDCl_3 at room temperature.

Fourier transform infrared spectroscopy (FTIR):

FTIR measurements were done on Perkin-Elmer Model 2000 FTIR using KBr pellet. Thirty scans were signal-averaged with a resolution of 8 cm^{-1} at ambient temperature.

Electron spray ionization low-resolution mass spectrometry (ESI-LRMS):

ESI-LRMS was done on Bruker Daltonics MicroTOF-Q-II mass spectrometer using acetonitrile as solvent.

Matrix-assisted laser desorption ionization (MALDI):

Matrix-assisted laser desorption ionization time of flight mass spectrometry was performed with Bruker Daltonics UltrafleXtreme, using software flexControl version 3.4.

Gel permeation chromatography (GPC):

The molecular weight of the soluble polymer was estimated by gel permeation chromatography (GPC, Polymer Laboratories). Polystyrene was used as the calibration standard. PLGel mixed D and mixed C columns were used. The eluent was THF (flow rate: 1 mL min^{-1} at $40\text{ }^\circ\text{C}$). The refractive index of the eluent: $n(c) = n_s + \frac{\partial n}{\partial c}c + \dots$, where, c is the concentration in g mL^{-1} of the eluting polymer, n_s is the refractive index of the solvent and $\frac{\partial n}{\partial c}$ is the refractive index increment. The refractive index of THF ($n_s = 1.404$) and $\frac{\partial n}{\partial c}$ of the polystyrene standard (0.185 mL g^{-1}) were used.

Thermogravimetric analysis (TGA):

TGA analysis was carried out using Perkin Elmer TGA-6000 instrument. The sample was heated at a rate of $10\text{ }^\circ\text{C min}^{-1}$ under a nitrogen atmosphere to a maximum of $800\text{ }^\circ\text{C}$.

Field emission scanning electron microscopy (FESEM):

The morphology of polymer was examined using Carl Zeiss (Ultraplus) field emission scanning electron microscope. The accelerating voltage of 5 kV and 20 kV were used.

High-resolution transmission electron microscopy (HRTEM):

The porous nature of CzBDP was observed through HRTEM using FEI TALOS 200S instrument at a working voltage of 200 kV .

BET analysis:

All the gas adsorption measurements were performed on Quantachrome Autosorb, QUA211011 equipment. The sample was degassed at 100 °C for 24 h under vacuum before analysis. Isotherms were analyzed using ASiQwin software.

Steady-state absorption spectroscopy:

UV-Visible absorption spectra were recorded on Cary 100 spectrophotometer using 10 mm path length quartz cuvette.

Steady-state fluorescence spectroscopy:

Steady-state fluorescence measurements were carried out on Jobin Yvon Horiba Model Fluorolog-3-21. All the fluorescence spectra were corrected with respect to the excitation light intensity and photomultiplier tube (PMT) response using the correction files available with Horiba software. The optical density of the samples was maintained low enough to avoid any inner filter effect.

Electron paramagnetic resonance (EPR):

EPR spectra were recorded on Bruker EMX MicroX spectrometer. The specific measurement details regarding the trapping of reactive oxygen species (ROS) is as follows: the modulation frequency = 100 kHz, modulation amplitude = 0.2 G. The samples were prepared by adding 100 µL of 2,2,6,6-tetramethylpiperidine (TEMP) or 5,5-dimethyl-1-pyrroline *N*-oxide (DMPO) to 300 µL of toluene or acetonitrile, respectively. Subsequently, the CPOPs were added to the above solution.

Cyclic voltammetry:

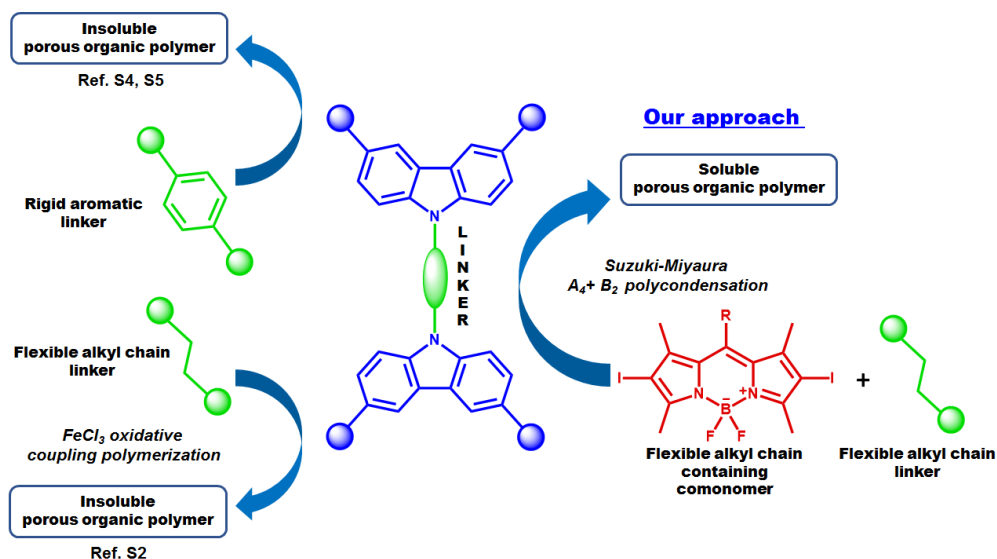
All electrochemical measurements were performed using CH instrument. An Ag/AgCl (3 M KCl) electrode as a reference electrode, glassy carbon as a working electrode and Pt wire as a counter electrode were used in a three-electrode cell. Tetrabutylammonium hexafluorophosphate (0.1 M) was used as a supporting electrolyte. All the experiments were performed at ambient temperature (25 ± 1 °C) under a nitrogen atmosphere.

Photooxidation:

Photooxidation experiments were carried out using a custom-made photoreactor with a 9 W household energy saving compact fluorescent lamp (CFL).

II. Design strategy for developing a smart photosensitizer based on soluble conjugated porous organic polymer (CPOP)

The soluble conjugated porous organic polymer, CzBDP is a new polymer (structurally novel) having a unique combination of interesting features like solution processability, π -electron conjugation, porosity, red emission and excellent capability of ROS generation. The separation of carbazole units by alkyl chain was demonstrated for the fabrication of blue fluorescent linear soluble electroactive polymer.¹ Insoluble porous polymer network based on carbazole–alkyl spacer–carbazole by FeCl_3 oxidative coupling polymerization was reported.² The copolymerization with simple alkyl substituted BODIPY, pristine carbazole or substituted carbazole, N,N' -bicarbazole and oxidative polymerization of carbazole-alkyl spacer-carbazole would lead to insoluble porous network.²⁻⁷ The key issue to maintain solution processability albeit imparting porosity is to separate the carbazole units by long alkyl chain (A_4 unit) followed by polymerization with a suitable comonomer (B_2 unit); in the present case, we used alkyl substituted BODIPY (Scheme S1). We believe that the most novel aspect of the present manuscript is the design strategy to circumvent the strong π - π stacking among aromatic building blocks and achieving solution processability as well as improved ROS generation capability in a network polymer.



Scheme S1 Schematic illustration demonstrating the design strategy for the fabrication of carbazole (Cz) and boron dipyrromethene (BODIPY) based soluble conjugated porous organic polymer (CzBDP) for the generation of reactive oxygen species (ROS).

III. Synthesis & characterization

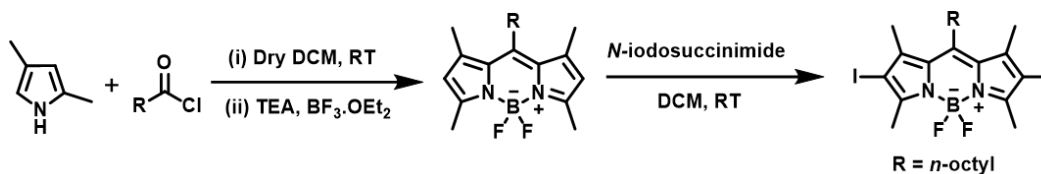
(a) Chemicals:

All chemicals were used as received unless stated otherwise. Carbazole (95 %), 1,8-dibromooctane (98 %), tetrabutylammonium bromide (98 %), cesium carbonate (99 %), 1,1'-ferrocenediyl-bis(diphenylphosphine) (97%), 1,1'-bis(diphenylphosphino) ferrocene dichloro palladium(II) (99%), dimethyl sulfoxide (99%) toluene (99.85%), diisopropylamine (99%), tetrakis(triphenylphosphine)palladium (99.9%), *N*-bromosuccinimide (99%), *N*-iodosuccinimide (99%), 2,4-dimethylpyrrole (97 %), nonanoylchloride (96%), boron trifluoride diethyl etherate (for synthesis), trimethylamine (99.5%), 2,7-dibromo-9H-carbazole (97%), benzylamine (99 %) were received from Sigma-Aldrich. Potassium hydroxide (99%), chloroform and hexane were received from Merck. THF (99%), ethanol (99.8%), extra pure concentrated HCl were received from Spectrochem.

(b) Synthesis and characterization of monomers

(i) Synthesis of 5,5-difluoro-2,8-diiodo-1,3,7,9-tetramethyl-10-octyl-5H-dipyrrolo diazaborinine

In a typical synthetic procedure, 2,4-dimethyl pyrrole (2 mL, 2 equiv.) and nonanoyl chloride (2.2 mL, 1 equiv.) were dissolved in dry DCM (25 mL). The solution was stirred at room temperature overnight followed by the addition of 3 mL of Et₃N and 3 mL of BF₃.OEt₂. After 30 min, the reaction mixture was washed with H₂O and dried over MgSO₄. The solvent was evaporated to dryness and the residue was purified by silica gel column chromatography to afford a red solid (Yield 20%).³



Scheme S2 Synthetic scheme of 5,5-difluoro-2,8-diiodo-1,3,7,9-tetramethyl-10-octyl-5H-dipyrrolo diazaborinine.

Iodination of BODIPY was carried out with *N*-iodosuccinimide (NIS). BODIPY (0.5 mmol) and NIS (2 mmol) were dissolved in dry DCM (15 mL). The mixture was stirred at room

temperature for 8 h. The solvent was removed under reduced pressure and the crude product was purified by silica gel column chromatography (Yield 35 %, Scheme S2).

¹H NMR (500 MHz, CDCl₃): δ 3.03 – 2.96 (m, 2H), 2.61 (s, 6H), 2.48 (s, 6H), 1.65 – 1.58 (m, 2H), 1.53 – 1.47 (m, 2H), 1.38 – 1.26 (m, 8H), 0.89 (t, *J* = 7.0 Hz, 3H).

¹³C NMR (126 MHz, CDCl₃): δ 155.2, 146.4, 142.2, 131.3, 86.3, 31.7, 31.7, 30.3, 29.7, 29.3, 29.2, 22.6, 18.9, 16.1, 14.0.

ESI-LRMS: Calculated for C₂₁H₂₉BF₂I₂N₂, 612.09, found 612.0.

(ii) Synthesis of 1,8-bis(carbazolyl)octane

9H-carbazole (1 mmol), 1,8-dibromooctane (0.5 mmol) and tetrabutylammonium bromide (0.2 mmol) were added together in 2 mL DMSO under stirring. Then the mixture was stirred for 5 min. An aqueous solution of KOH (50%) was added drop wise to the reaction mixture and heated at 80 °C for 2 h. The reaction mixture was cooled to room temperature and was quenched with water and was subsequently extracted with DCM (3 × 10 mL). Then the organic part was concentrated and purified with column chromatography (silica gel) to afford 1,8-bis(carbazolyl)octane (Yield 80 %, Scheme S3).



Scheme S3 Synthetic scheme of 1,8-bis(carbazolyl)octane.

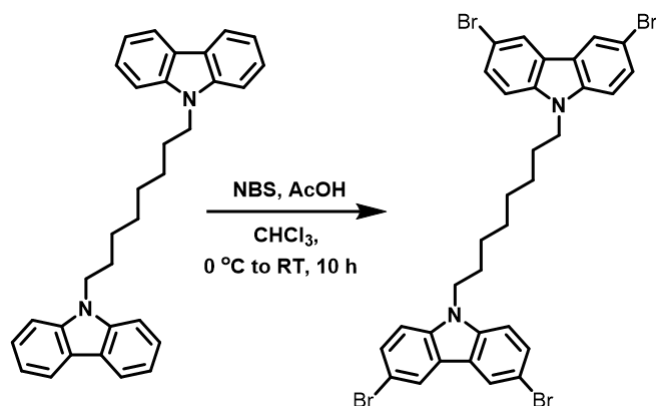
¹H NMR (500 MHz, CDCl₃): δ 8.09 (d, *J* = 7.8 Hz, 4H), 7.45 (t, *J* = 7.6 Hz, 4H), 7.38 (d, *J* = 8.2 Hz, 4H), 7.22 (t, *J* = 7.0 Hz, 4H), 4.26 (t, *J* = 7.2 Hz, 4H), 1.87 – 1.81 (m, 4H), 1.33 – 1.23 (m, 8H).

¹³C NMR (126 MHz, CDCl₃): δ 140.4, 125.6, 122.8, 120.3, 118.7, 108.6, 43.0, 29.2, 28.8, 27.1.

MALDI-TOF: Calculated for C₃₂H₃₂N₂, 444.6, found 444.1.

(iii) Synthesis of 1,8-bis(3,6-dibromo-9H-carbazol-9-yl)octane

In a 50 mL round-bottom flask covered with aluminium foil, 1,8-bis(carbazolyl)octane (200 mg, 0.45 mmol) was dissolved in 5 mL chloroform and acetic acid (3:2 v/v ratio) at 0 °C. Then *N*-bromosuccinimide (354 mg, 2.0 mmol) was added at once to the reaction mixture and allowed to stir for 5 min. Then, the reaction mixture was allowed to stir at room temperature for 10 h. The solvent was removed under reduced pressure and the crude product was purified by column chromatography (silica gel) using hexane as eluent (Yield 70 %, Scheme S4).



Scheme S4 Synthetic scheme of 1,8-bis(3,6-dibromo-9H-carbazol-9-yl)octane.

¹H NMR (500 MHz, CDCl₃): δ 8.14 (d, $J = 1.9$ Hz, 4H), 7.54 (dd, $J = 8.7, 1.9$ Hz, 4H), 7.23 (d, $J = 8.7$ Hz, 4H), 4.20 (t, $J = 7.1$ Hz, 4H), 1.82 – 1.72 (m, 4H), 1.24 (d, $J = 19.3$ Hz, 8H).

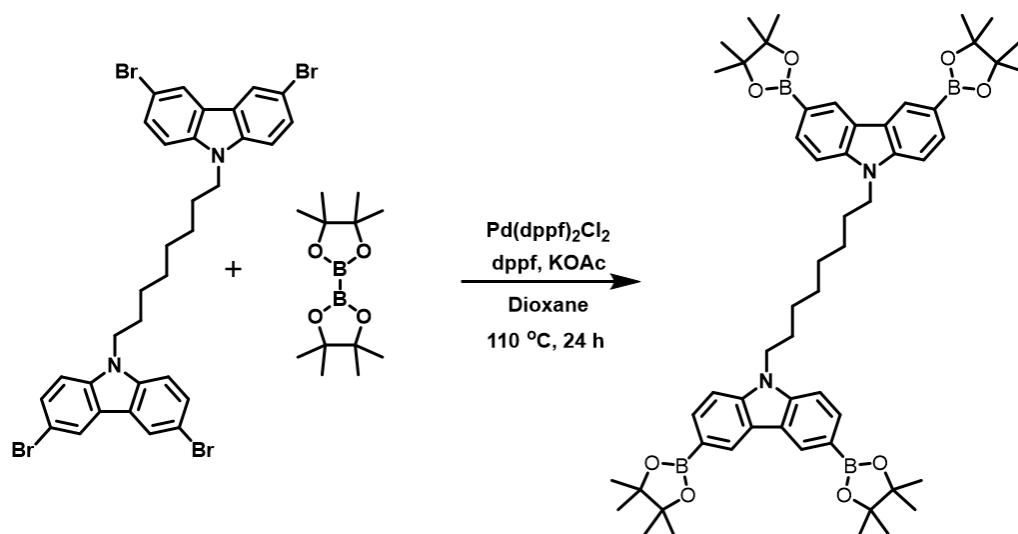
¹³C NMR (126 MHz, CDCl₃): δ 139.3, 129.0, 123.5, 123.3, 111.9, 110.4, 43.3, 29.1, 28.7, 27.0.

MALDI –TOF: Calculated for C₃₂H₂₈Br₄N₂, 760.2, found 760.0.

(iv) Synthesis of 1,8-bis(3,6-bis(4,4,5,5-tetramethyl-1,3,2-dioxaborolan-2-yl)-9H-carbazol-9-yl)octane (TDCO)

In a 50 mL Schlenk tube 1,8-bis(3,6-dibromo-9H-carbazol-9-yl)octane (1 mmol, 1 equiv.), bis(pinacolato)diboron (5 mmol, 5 equiv.), potassium acetate (8 mmol, 8 equiv.) 1,1'-bis(diphenylphosphino)ferrocenepalladium(II) dichloride (10 mol%) and 1,1'-bis(diphenylphosphino)ferrocene (10 mol%) in dioxane (10 mL) were refluxed at 110 °C under argon atmosphere for 24 h. The reaction mixture was cooled to room temperature and was quenched with water and extracted with dichloromethane (3 × 10 mL). The combined organic layer was dried over anhydrous MgSO₄. The organic solvent was evaporated and the crude product

was purified by column chromatography (silica gel) using a mixture of hexane and ethyl acetate as eluent (Yield 40 %, Scheme S5).



Scheme S5 Synthetic scheme of 1,8-bis(3,6-bis(4,4,5,5-tetramethyl-1,3,2-dioxaborolan-2-yl)-9H-carbazol-9-yl)octane.

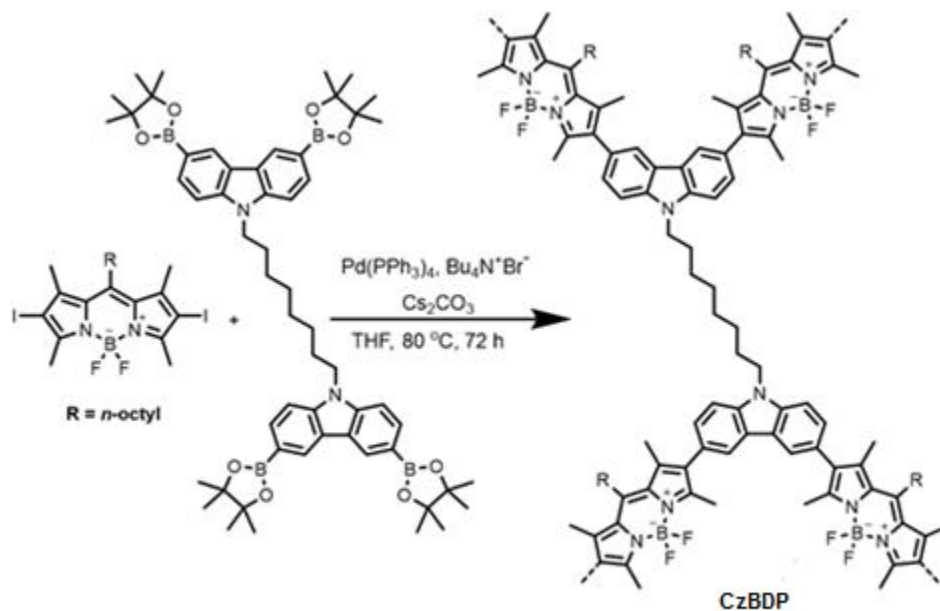
¹H NMR (500 MHz, CDCl₃): δ 8.68 (s, 4H), 7.92 (d, J = 8.1 Hz, 4H), 7.39 (d, J = 8.2 Hz, 4H), 4.29 (t, J = 7.2 Hz, 4H), 1.98 – 1.72 (m, 4H), 1.41 (s, 32H), 1.29 (s, 24H).

MALDI –TOF: Calculated for C₅₅H₇₂B₄N₂O₈, 948.5, found 948.7.

(c) Fabrication of the soluble porous polymer (CzBDP)

The polymer CzBDP was synthesized by Pd-catalyzed Suzuki-Miyaura cross-coupling polycondensation reaction between the monomer 1,8-bis(3,6-bis(4,4,5,5-tetramethyl-1,3,2-dioxaborolan-2-yl)-9H-carbazol-9-yl)octane (TDCO) and comonomer 2,8-diiodo-BODIPY. In a typical synthetic procedure, TDCO (1 mmol), 2,8-diiodo-BODIPY (2 mmol), tetrakis(triphenylphosphine)palladium (0) (10 mol %), tetrabutylammonium bromide (50 mg) were taken in a Schlenk tube. 20 mL of dry THF was added and was subjected to freeze-pump-thaw cycles to remove the dissolved oxygen. 2 mL of a degassed aqueous solution of cesium carbonate (2 M) was added to the mixture. The reaction mixture was stirred for 72 h at 80 °C under an argon atmosphere and protected from light. The reaction mixture was cooled down to room temperature and then diluted with 100 mL of chloroform and 100 mL of water and successively extracted three times with 50 mL of chloroform. The organic phase was washed with 100 mL of 1 M hydrochloric acid followed by a saturated aqueous solution of sodium bicarbonate and aqueous EDTA solution and finally with water. The organic part was dried over anhydrous MgSO₄ and

filtered. The solvent was removed under reduced pressure. The residue was dissolved in small amount of chloroform and precipitated into the ultra-cold methanol. The precipitate was washed with methanol and acetone, and then was washed thoroughly by Soxhlet extraction for 24 h successively, with methanol and acetone and was dried under vacuum at 80 °C to obtain the pure polymer (Yield 30 to 35 %, Scheme S6).

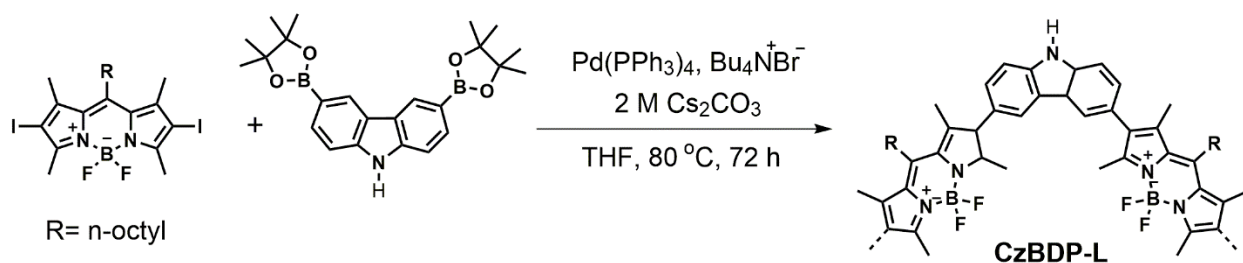


Scheme S6 Fabrication of soluble conjugated porous organic polymer CzBDP.

(d) Fabrication of the soluble linear polymer (CzBDP-L)

The soluble linear polymer CzBDP-L was synthesized by Pd-catalyzed Suzuki-Miyaura cross-coupling polycondensation reaction between the monomer 3,6-bis(4,4,5,5-tetramethyl-1,3,2-dioxaborolan-2-yl)-9H-carbazole and comonomer 2,8-diiodo-BODIPY. During the synthesis, 1 mmol monomer, 1 mmol comonomer, tetrakis(triphenylphosphine)palladium (0) (10 mol %), tetrabutylammonium bromide (50 mg) were taken in a Schlenk tube. 20 mL of dry THF was added and was subjected to freeze-pump-thaw cycles to remove the dissolved oxygen. 2 mL of a degassed aqueous solution of cesium carbonate (2 M) was added to the mixture. The reaction mixture was stirred for 72 h at 80 °C under an argon atmosphere and protected from light. The reaction mixture was cooled down to room temperature and then diluted with 100 mL of chloroform and 100 mL of water and successively extracted three times with 50 mL of chloroform. The organic phase was washed with 100 mL of 1 M hydrochloric acid followed by a saturated

aqueous solution of sodium bicarbonate and aqueous EDTA solution and finally with water. The organic part was dried over anhydrous MgSO_4 and filtered. The solvent was removed under reduced pressure. The residue was dissolved in small amount of chloroform and precipitated into the ultra-cold methanol. The precipitate was washed with methanol and acetone, and then was washed thoroughly by Soxhlet extraction for 24 h successively, with methanol and acetone and was dried under vacuum at $80\text{ }^\circ\text{C}$ to obtain the pure polymer (Yield 50 %, Scheme S7).



Scheme S7 Fabrication of soluble linear polymer CzBDP-L.

(e) Characterization of the soluble porous polymer (CzBDP)

(i) Fourier transform infrared (FTIR) spectroscopy

Fig. S1 is a comparison of FTIR spectra of the monomers along with the CzBDP polymer. It is noticeable that the aliphatic C–H stretching (2850 cm^{-1} , 2925 cm^{-1}) band was present in the polymer and as well as in the monomers. The aromatic C–H stretching (3050 cm^{-1}) observed in case of TDCO core and the CzBDP. The 1548 cm^{-1} band of CzBDP is assignable to the C=N stretching of the BDP unit.

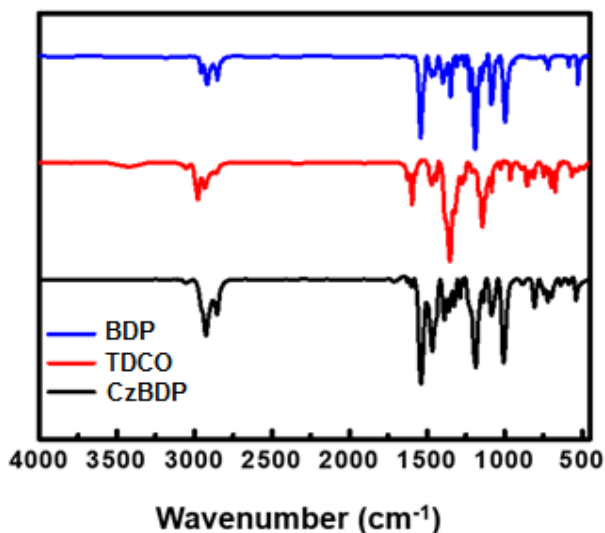


Fig. S1 FTIR spectra of substituted BODIPY (BDP), boronic ester of carbazole-di octane (TDCO) and CzBDP polymer.

(ii) Nuclear magnetic resonance (NMR) spectroscopy

The ^1H NMR spectrum of CzBDP was compared with that of the constituent monomers, clearly indicating similar resonances in addition to other resonances demonstrating polycondensation between the monomers (Fig. S2).

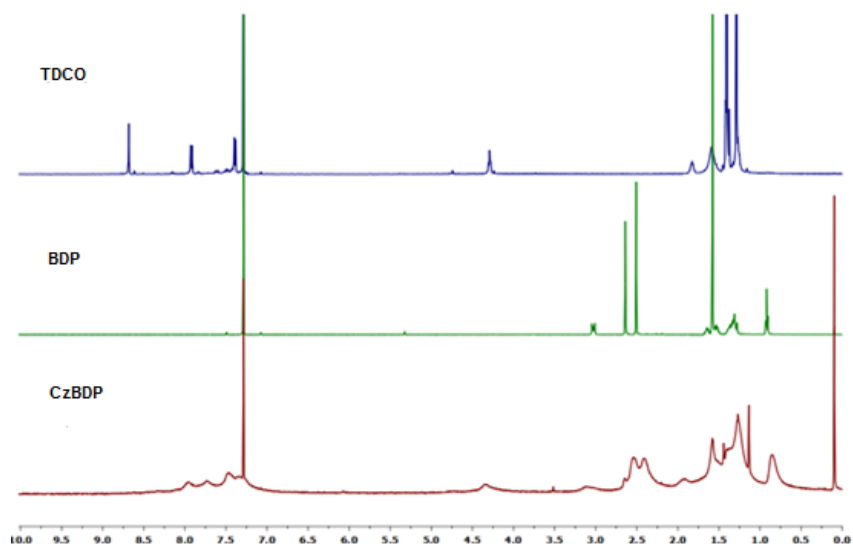


Fig. S2 ^1H NMR spectra of CzBDP, BDP and TDCO in CDCl_3 at room temperature.

(iii) Gel permeation chromatography (GPC) analysis

The molar mass of CzBDP was found to be $M_w \sim 18400 \text{ g mol}^{-1}$ with the polydispersity index of 1.4 (Fig. S3), as estimated by gel permeation chromatography (GPC). Polystyrene was used as the calibration standard. THF was used as the eluent (flow rate: 1 mL min^{-1} at 40°C). The universal calibration was used employing refractive index and viscometry detectors.

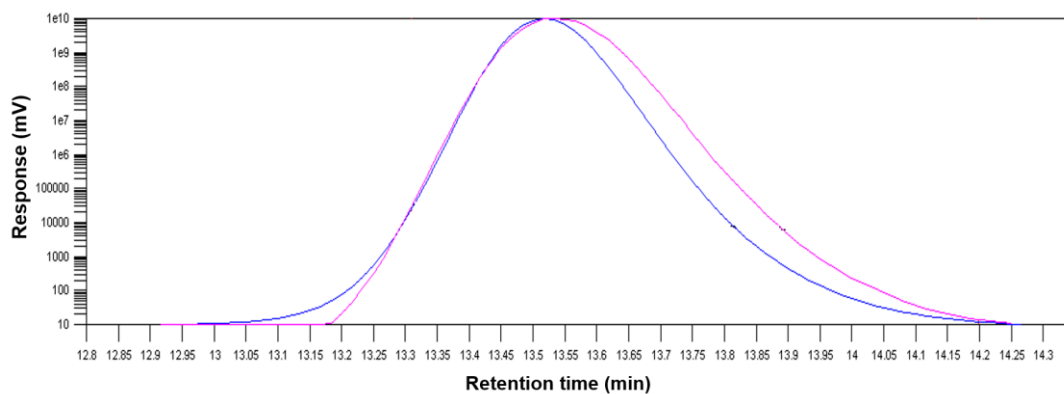


Fig. S3 GPC chromatograms of CzBDP (blue: refractive index and magenta: viscometry detector).

(iv) Thermogravimetric analysis (TGA)

TGA analysis was carried out using Perkin Elmer TGA-6000 instrument. CzBDP was heated at a rate of $10\text{ }^{\circ}\text{C min}^{-1}$ under a nitrogen atmosphere to a maximum of $800\text{ }^{\circ}\text{C}$. Fig. S4 depicts that CzBDP was stable upto $300\text{ }^{\circ}\text{C}$.

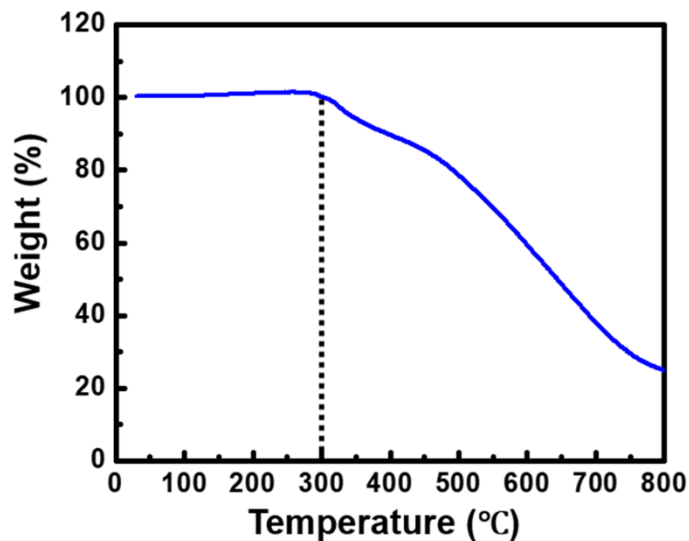


Fig. S4 TGA-plot of CzBDP (scan rate $10\text{ }^{\circ}\text{C min}^{-1}$ under N_2).

(f) Characterization of the soluble linear polymer (CzBDP-L)

(i) Fourier transform infrared (FTIR) spectroscopy

Fig. S5 depicts the comparison of FTIR spectra of the monomers along with the CzBDP-L polymer. It was noticeable that the aliphatic C–H stretching (2860 cm^{-1} , 2926 cm^{-1}) band was present in the polymer as well as in the monomers. The broad N–H stretching (3402 cm^{-1}) observed in case of Cz core and the CzBDP-L. The 1540 cm^{-1} band of CzBDP-L is assignable to the C=N stretching of the BDP unit.

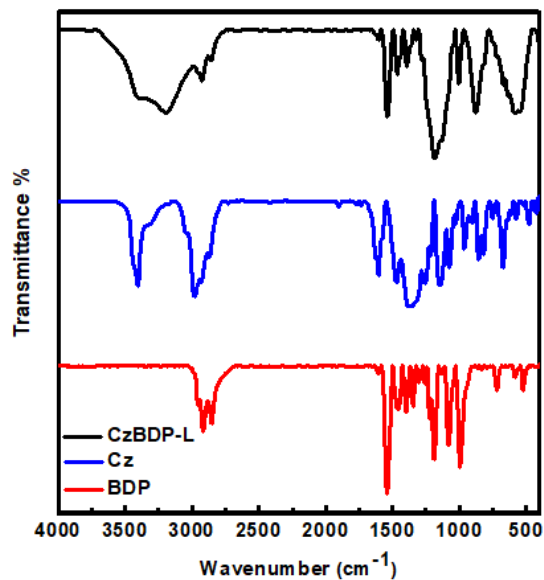


Fig. S5 FTIR spectra of substituted BODIPY (BDP), boronic ester of carbazole (Cz) and CzBDP-L polymer.

(ii) Nuclear magnetic resonance (NMR) spectroscopy

The ^1H NMR spectrum of CzBDP-L was compared with that of the constituent monomers, clearly indicating similar resonances in addition to other resonances demonstrating polycondensation between the monomers (Fig. S6).

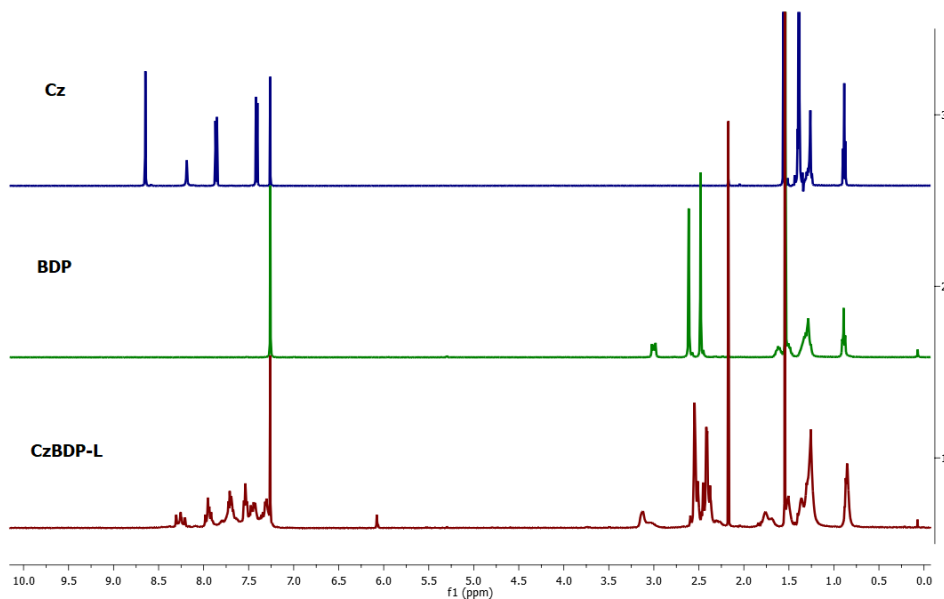


Fig. S6 ^1H NMR spectra of CzBDP-L, BDP and Cz in CDCl_3 (298 K).

(g) Microscopic characterizations

(i) CzBDP porous polymer:

Samples for FESEM were prepared by sprinkling (~ 2 mg) powdered polymers on the aluminium stub using the adhesive carbon tape. All samples were coated with a thin layer of sputtered gold before imaging. The FESEM images reveal the sphere like morphology of the CzBDP polymer (Fig. S7).

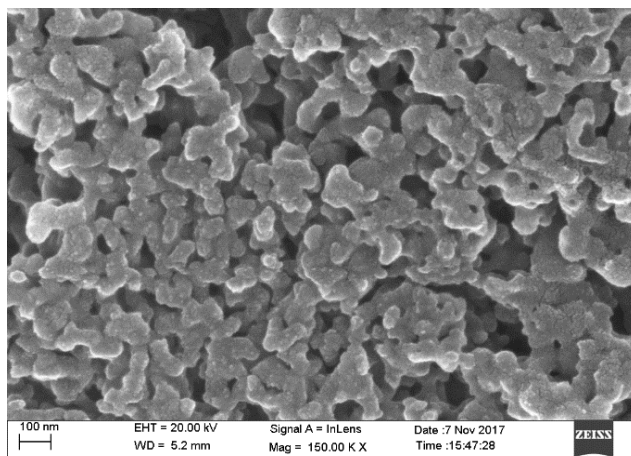


Fig. S7 FESEM image of CzBDP polymer.

HRTEM samples were prepared by drop casting a homogeneous dilute dispersion of CzBDP polymer (in ethanol) over a carbon coated 400 mesh Cu grid. The HRTEM images also corroborated the porous nature of CzBDP (Fig. S8).

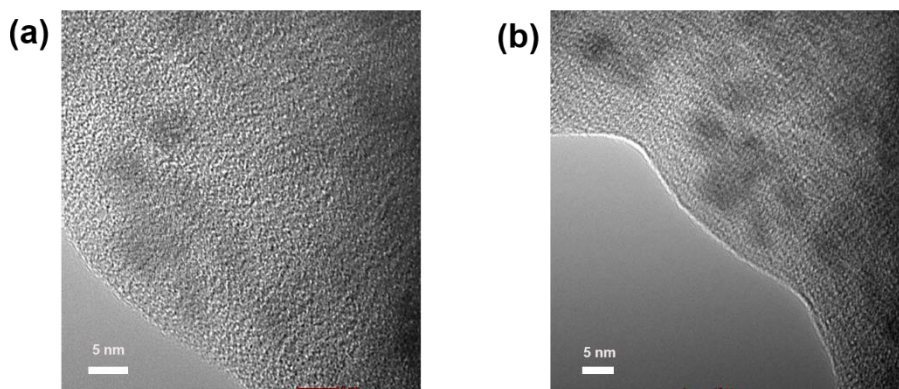


Fig. S8 HRTEM images of CzBDP polymer.

(ii) CzBDP-L linear polymer:

Samples for FESEM were prepared by sprinkling (~ 2 mg) powdered polymers on the aluminium stub using the adhesive carbon tape. All samples were coated with a thin layer of sputtered gold before imaging. The FESEM images reveal the sphere like morphology of the CzBDP-L polymer (Fig. S9).

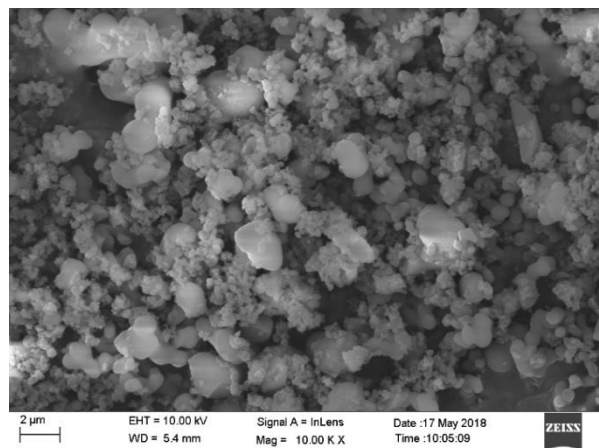


Fig. S9 FESEM image of CzBDP-L polymer.

IV. Gas sorption

Samples were degassed at 100 °C for 24 h under vacuum before analysis. Nitrogen adsorption-desorption isotherms were measured at 77 K. The surface area and pore size distributions were estimated by nitrogen adsorption-desorption isotherms (Fig. S10, Table S1). Pore size distributions were derived from nonlocal density functional theory (NLDFT) method.⁸

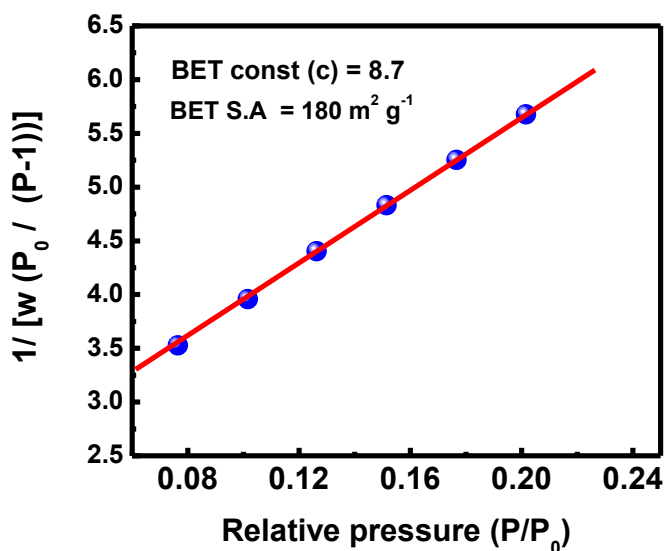


Fig. S10 BET specific surface area plot of CzBDP with the relative pressure range $0.08 < P/P_0 < 0.2$.

Table S1 Surface properties of CzBDP based on nitrogen sorption measurement.

Sample	BET (m ² g ⁻¹)	Pore size (nm)	Pore volume (cc g ⁻¹) [#]
CzBDP	180	2.8 and 4.4	0.26

[#] P/P₀ = 0.95

V. Spectroscopic investigation

Steady-state spectroscopy

The Steady-state absorption, fluorescence emission and fluorescence excitation measurements of 1,8-bis(carbazolyl)octane, alkylated BODIPY, CzBDP and CzBDP-L polymer were carried out in tetrahydrofuran. Fig. S11 depicts the normalized absorption, emission and excitation spectra of CzBDP.

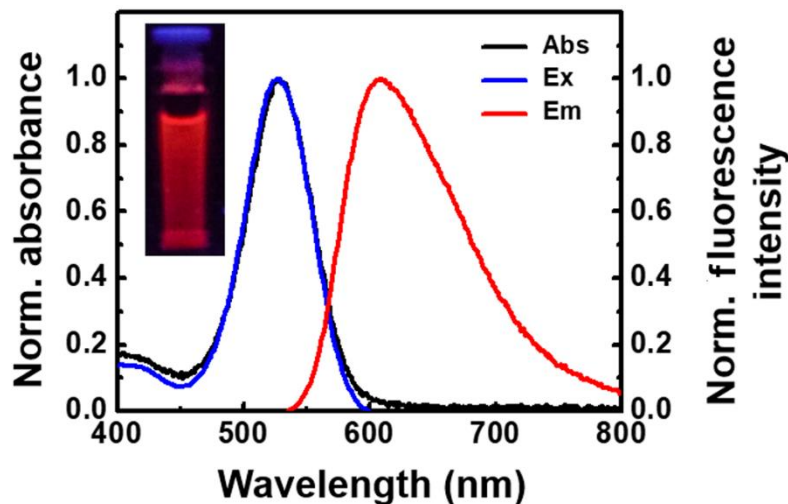


Fig. S11 Normalized absorption, emission ($\lambda_{exc} = 530$ nm) and excitation ($\lambda_{em} = 610$ nm) spectra of CzBDP in THF. Inset: The photograph of a THF solution of CzBDP under the irradiation of UV light at 365 nm.

The normalized absorption, emission and excitation spectra of substituted carbazole and BODIPY are shown in Fig. S12. The absorption maximum of the CzBDP polymer was found to be red shifted (530 nm) than that of substituted carbazole (350 nm) and BODIPY (498 nm).

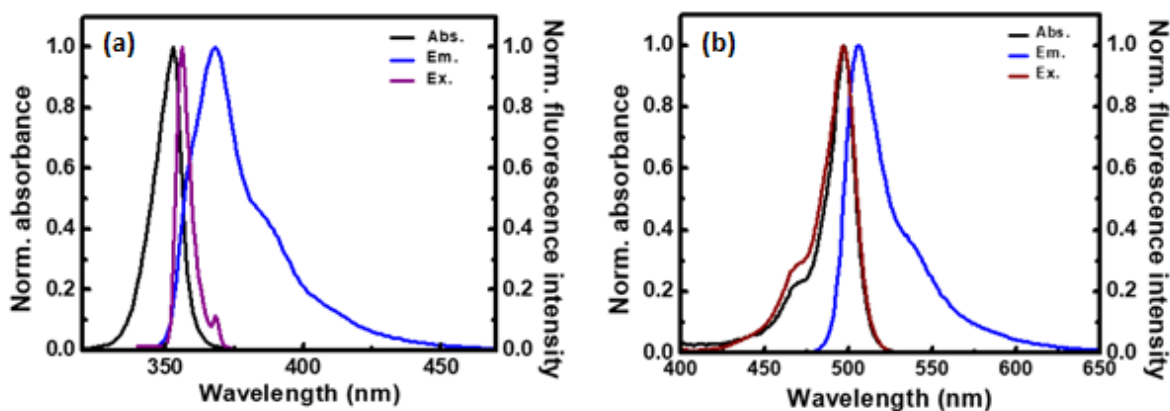


Fig. S12 (a) Absorption, emission ($\lambda_{exc} = 350$ nm) and excitation spectra ($\lambda_{em} = 370$ nm) of 1,8-bis(carbazolyl)octane. (b) Absorption, emission ($\lambda_{exc} = 498$ nm) and excitation spectra ($\lambda_{em} = 508$ nm) of BODIPY.

The emission band of CzBDP (610 nm, Fig. S11) as well as CzBDP-L (595 nm, Fig. S13) were significantly red-shifted compared to substituted carbazole (370 nm) and BODIPY (510 nm). The red shifts in absorption and emission of CzBDP and CzBDP-L compared to those of the monomeric units are presumably due to the extended π -electron conjugation throughout the polymer backbone (Table S2).

Table S2 Spectroscopic data of the polymer and monomers in tetrahydrofuran.

Sample	λ_{\max} (abs)	λ_{\max} (em)	λ_{\max} (exc)
1,8-bis(carbazolyl)octane	350	370	356
Alkylated BODIPY	498	508	498
CzBDP	530	610	530
CzBDP-L	527	595	528

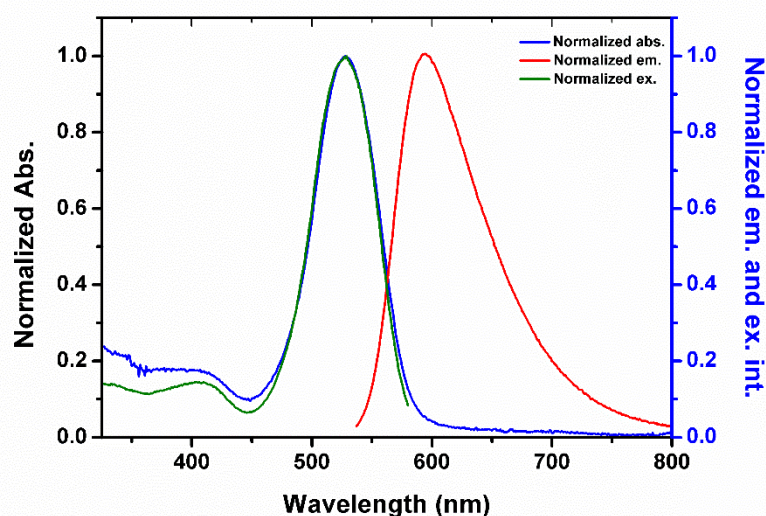


Fig. S13 Absorption, emission ($\lambda_{\text{exc}} = 527$ nm) and excitation spectra ($\lambda_{\text{em}} = 595$ nm) of CzBDP-L.

Fluorescence quantum yield (ϕ_f) measurement

The fluorescence quantum yield of CzBDP (THF) was estimated in comparison with the standard Rhodamine B solution in EtOH ($\phi_f = 0.7$). The quantum yield was calculated using the following equation.⁹

$$\Phi_{f,x} = \Phi_{f,s} \cdot \frac{F_x}{F_s} \cdot \frac{f_s}{f_x} \cdot \frac{n_x^2}{n_s^2}$$

where, Φ_f is fluorescence quantum yield, subscript x denotes the unknown sample (CzBDP) and subscript s refers to the standard dye. F denotes integral fluorescence, n refers to the refractive index of the solvent used in the measurements and f is the absorption factor at the excitation wavelength given by the following equation:

$f = 1 - 10^{-\varepsilon(\lambda_{ex})cl} = 1 - 10^{-A(\lambda_{ex})}$, where A is absorbance and ε = molar extinction coefficient in $\text{L mol}^{-1} \text{cm}^{-1}$.

VI. Cyclic voltammetry analysis

All electrochemical measurements were performed using CH instrument. In a typical electrochemical measurement, Ag/AgCl (3 M KCl) electrode was used as a reference electrode, glassy carbon was used as a working electrode and Pt wire was used as a counter electrode in a three-electrode cell. Tetrabutylammonium hexafluorophosphate (0.1 M) was used as a supporting electrolyte. All the experiments were performed at ambient temperature ($\sim 25^\circ\text{C}$) under a nitrogen atmosphere. The onset oxidation potential of CzBDP polymer in acetonitrile was found to be 0.96 V and the on-set reduction potential was -1 V (Fig. S14).

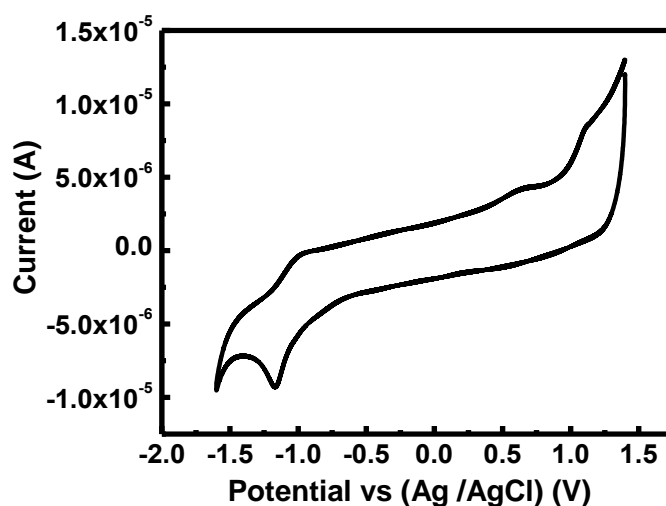
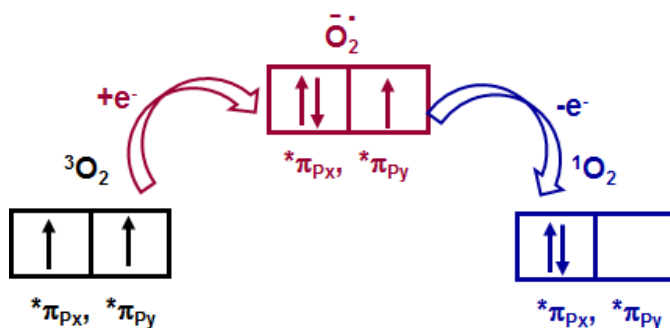


Fig. S14 Cyclic voltammogram of CzBDP in DCM; scan rate 10 mV s^{-1} .

VII. Generation of reactive oxygen species

(a) Mechanistic overview on reactive oxygen species generation

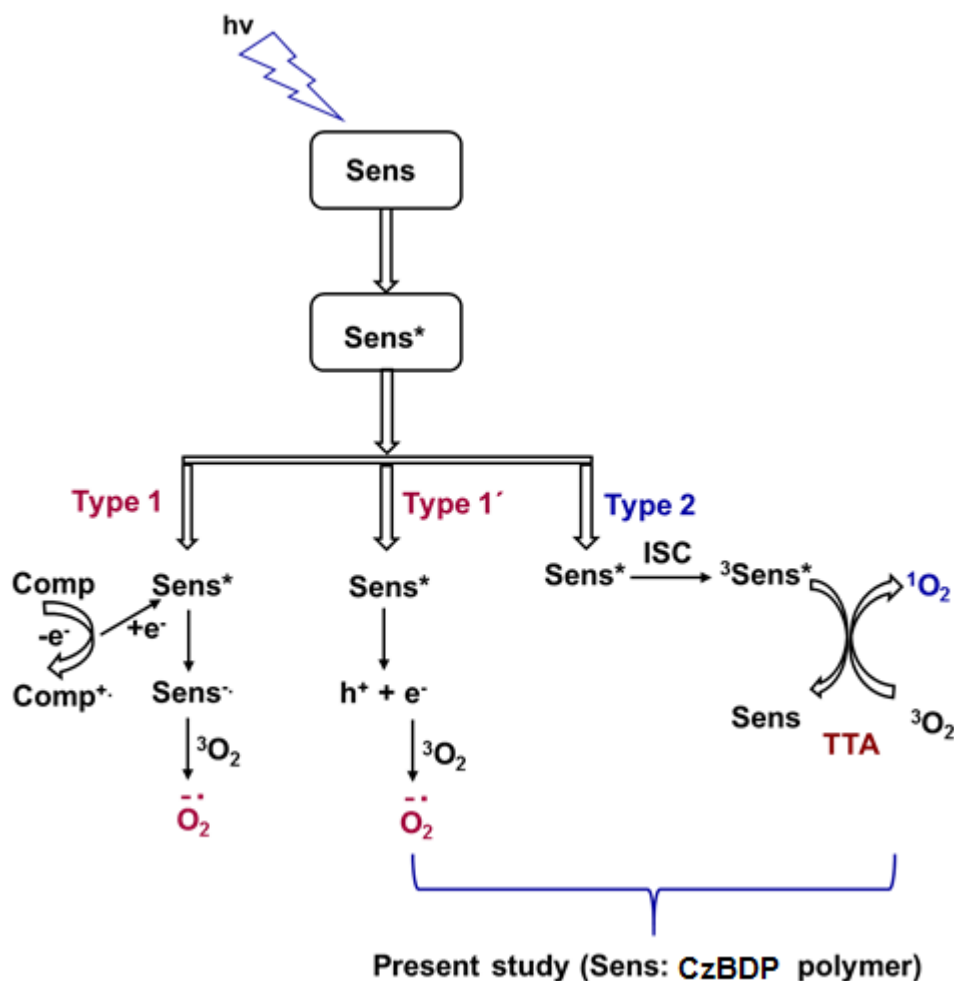
Molecular oxygen is a very important gaseous species on earth due to its enormous utilization for several kinds of biochemical processes in almost all living organisms. The quantum mechanics and the molecular orbital theory reveal that due to the presence of two unpaired electrons in highly energetic antibonding orbital makes the molecular oxygen reactive even at the ground state. Hence, the molecular oxygen can easily be converted to other reactive derivatives, called reactive oxygen species (ROS), through different transformations (Scheme S8).¹⁰ This chemical transformations of molecular oxygen to ROS can be assisted by different functional materials (small molecules, nanocomposites, porous graphene oxide, carbon nitride etc.) depending on their special structure-property relationships.¹¹⁻¹³ We found that the soluble conjugated porous organic polymer CzBDP is prone to the generation of singlet oxygen as well as superoxide anion radical upon photoexcitation. The reactivity of these two ROS makes them not only popular in the field of biological applications but also for photooxidation of toxic molecules as well as in photochemical synthesis.^{14,15}



Scheme S8 Frontier molecular π^* orbitals of molecular oxygen, superoxide anion radical and singlet oxygen.

A photosensitizer is often required for the generation of ROS as direct conversion of molecular oxygen to ROS upon photoexcitation is not allowed according to the spin selection rule.¹⁶ Photosensitizer absorbs light and induces photosensitization of ROS. There are two distinct pathways known for photosensitization, Type 1 and Type 2 (Scheme S9).^{17,18} In the case of Type 1, the photoexcited sensitizer (Sens^*) accepts an electron from the other component (Comp) of the system and leads to the formation of sensitizer and component radicals (Sens^\cdot and Comp^+), respectively. The sensitizer anion radical transfer one electron to the molecular oxygen and

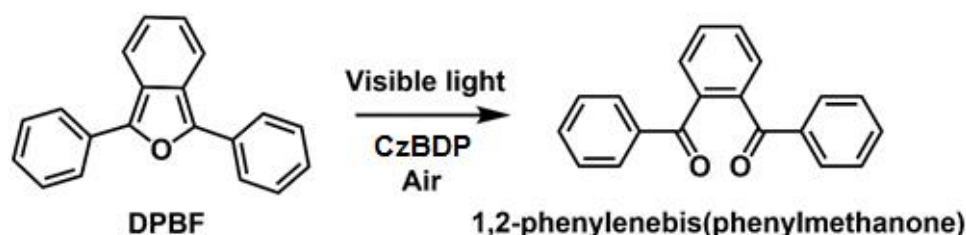
generates superoxide anion radical. The same phenomenon happens if the sensitizer can generate hole and electron pair during the photoexcitation (Type 1'). The photogenerated electron upon reacting with molecular oxygen produces the superoxide anion radical.¹⁹ On the other hand, the Type 2 mechanism is governed by the transfer of excitation energy of the photosensitizer (triplet state) to the ground state of molecular oxygen (3O_2) which leads to the formation of singlet oxygen (1O_2). This process is known as triplet-triplet annihilation (TTA).²⁰ The comparable band gap of the photosensitizer with the energy gap between molecular and singlet oxygen plays an important role for the successful TTA.²¹ The band gap measurement of CzBDP reveals that it is well capable for the generation of both $O_2^{\cdot-}$ and 1O_2 .



Scheme S9 Schematic illustration of various pathways of reactive oxygen species (ROS) generation.

(b) Generation of singlet oxygen

The generation of singlet oxygen by CzBDP with photoirradiation was probed through UV-Vis and EPR experiments. The time-dependent UV-Vis absorption experiment was carried out using 1,3-diphenylisobenzofuran (DPBF) which is a well-known singlet oxygen trapper.²² DPBF gets converted to its corresponding oxidized form through a peroxy intermediate in the presence of 1O_2 (Scheme S10).²³ The UV-Vis experiment for the probing of 1O_2 was carried out employing 50 μ M of 3 mL DPBF solution in DMF (maintaining the optical density (O.D) around 2.5 at 410 nm) and 50 μ L CzBDP solution in THF (1 mg mL⁻¹). In a typical experimental procedure, the above-mentioned solutions of DPBF and CzBDP were taken in a cuvette and the absorption maximum of DPBF was monitored upon irradiation at 530 nm (excitation of CzBDP) using a green LED (Fig. 2a, Main text). All the UV-Vis experiments were carried out avoiding exposure to ambient light as far as possible. The role of CzBDP polymer for the generation of singlet oxygen and subsequent degradation of the DPBF dye was probed by photoirradiation for different time intervals of (i) DPBF solution without CzBDP and (ii) DPBF solution with CzBDP. In the first case, we found that the DPBF dye was stable under the experimental condition whereas a significant photodegradation of the dye was observed in the presence of CzBDP (Fig. S15). This result indicates that the photodegradation of DPBF is due to the oxidation by 1O_2 obtained through photoirradiation of CzBDP polymer.



Scheme S10 The photochemical conversion of DPBF dye in the presence of singlet oxygen.

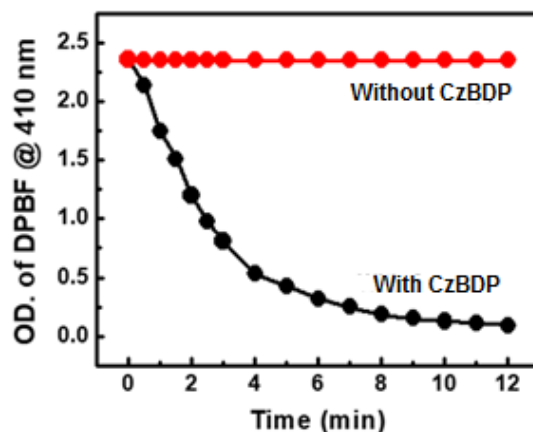


Fig. S15 The role of CzBDP polymer on the photochemical conversion of DPBF dye.

1O_2 generation capability of CzBDP porous polymer in solution was compared with alkylated BODIPY, iodinated alkylated BODIPY and linear conjugated polymer, CzBDP-L. All the experiments were carried out under the similar experimental conditions as that with the CzBDP polymer. The experimental results revealed that the alkylated BODIPY was unable to generate the 1O_2 (Fig. S16a) whereas, iodinated alkylated BODIPY showed a higher efficacy of 1O_2 generation (Fig. S16b, S16c) but the photostability became an important issue (Fig. S16d) as is the usual case with BODIPY-based small molecules.

The soluble porous polymer (CzBDP) was found to be more efficient 1O_2 generator as compared to that of its linear counterpart (CzBDP-L, Fig. S17). It is well established that the conjugated linear polymer suffers aggregation due to the strong π - π stacking interactions between aromatic building blocks, especially at high local concentrations.²⁴ It leads to self-quenching of

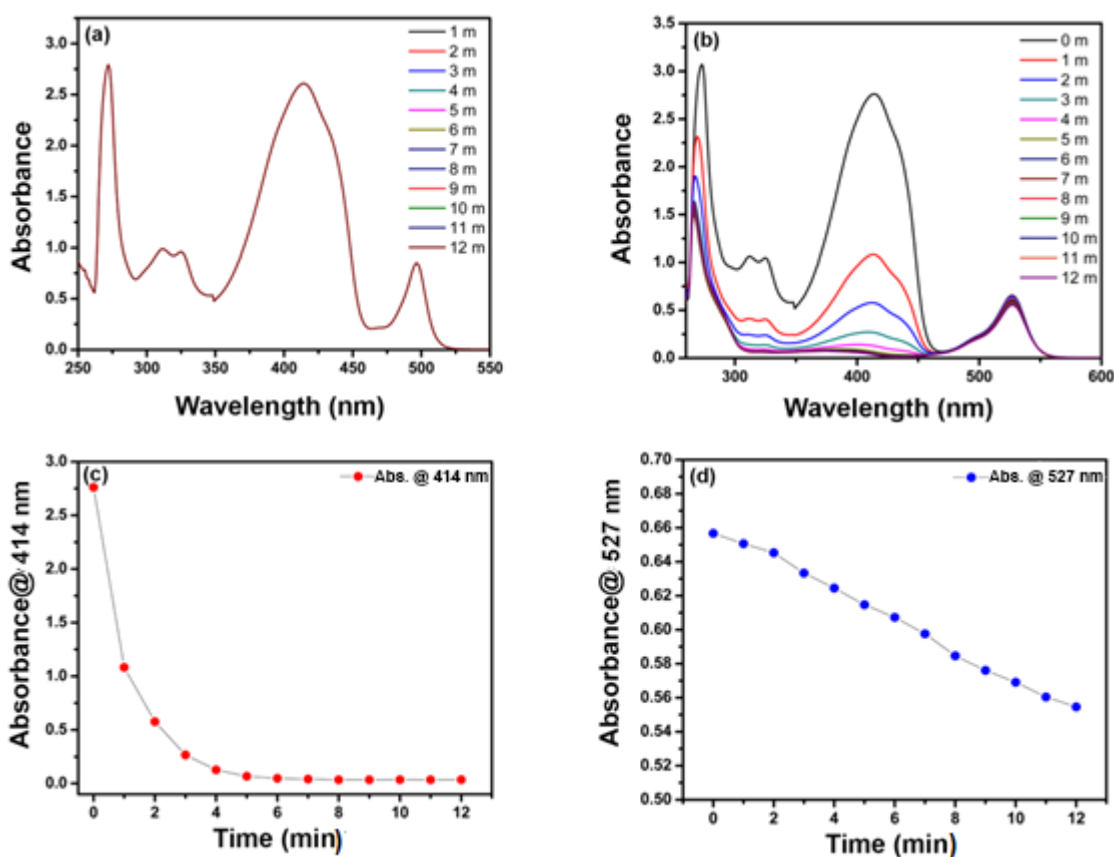


Fig. S16 Time-dependent absorption spectra of 1,3-diphenylisobenzofuran (DPBF) in DMF (3 mL, 50 μ M)) for probing the 1O_2 generation capability in the presence of (a) alkylated BODIPY and (b) iodinated alkylated BODIPY upon irradiation with a green LED at 530 nm. (c) Degradation kinetics of DPBF in the presence of iodinated alkylated BODIPY and (d) degradation of iodinated alkylated BODIPY under the experimental conditions.

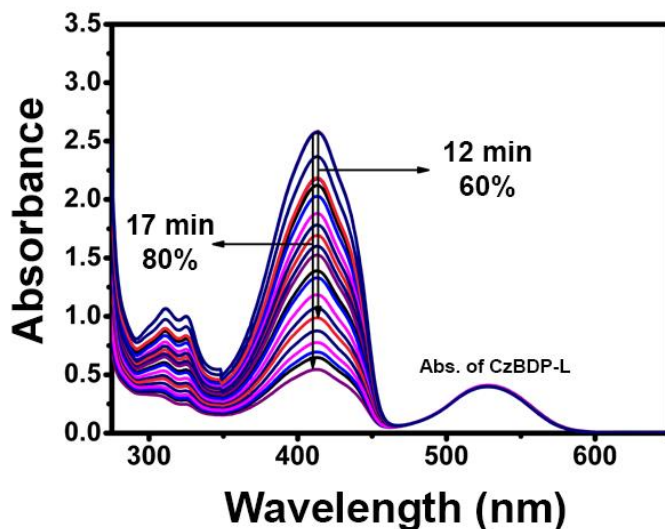


Fig. S17 Time-dependent absorption spectra of 1,3-diphenylisobenzofuran (DPBF) in DMF (3 mL, 50 μM) for probing the $^1\text{O}_2$ generation capability in the presence of CzBDP-L (50 μL , 1 mg mL^{-1}) upon irradiation with a green LED at 530 nm.

the excited state reducing the ability for $^1\text{O}_2$ generation.²⁵ Evidently, efficiency of CzBDP-L (50 μL , 1 mg mL^{-1} ; DPBF degradation: 60% in 12 min) for $^1\text{O}_2$ generation is lower than porous CzBDP (50 μL , 1 mg mL^{-1} ; DPBF degradation: 92% in 12 min) where branched structure and long alkyl chain between aromatic building blocks reduce π -stacking and provides more active sites for the interaction with molecular oxygen.²²

Solid dispersion of CzBDP in methanol and CzBDP thin films could also generate $^1\text{O}_2$ under photoirradiation. DPBF (3 mL, 50 μM in methanol) degradation by CzBDP (1 mg) dispersion was found to be 60% in 12 min (Fig. 18a). Fig. S18b reveals that CzBDP thin film is also capable for the generation of $^1\text{O}_2$. The time-dependent absorption study of CzBDP thin film indicated the photostability of the film under the experimental conditions (Fig. S18c).

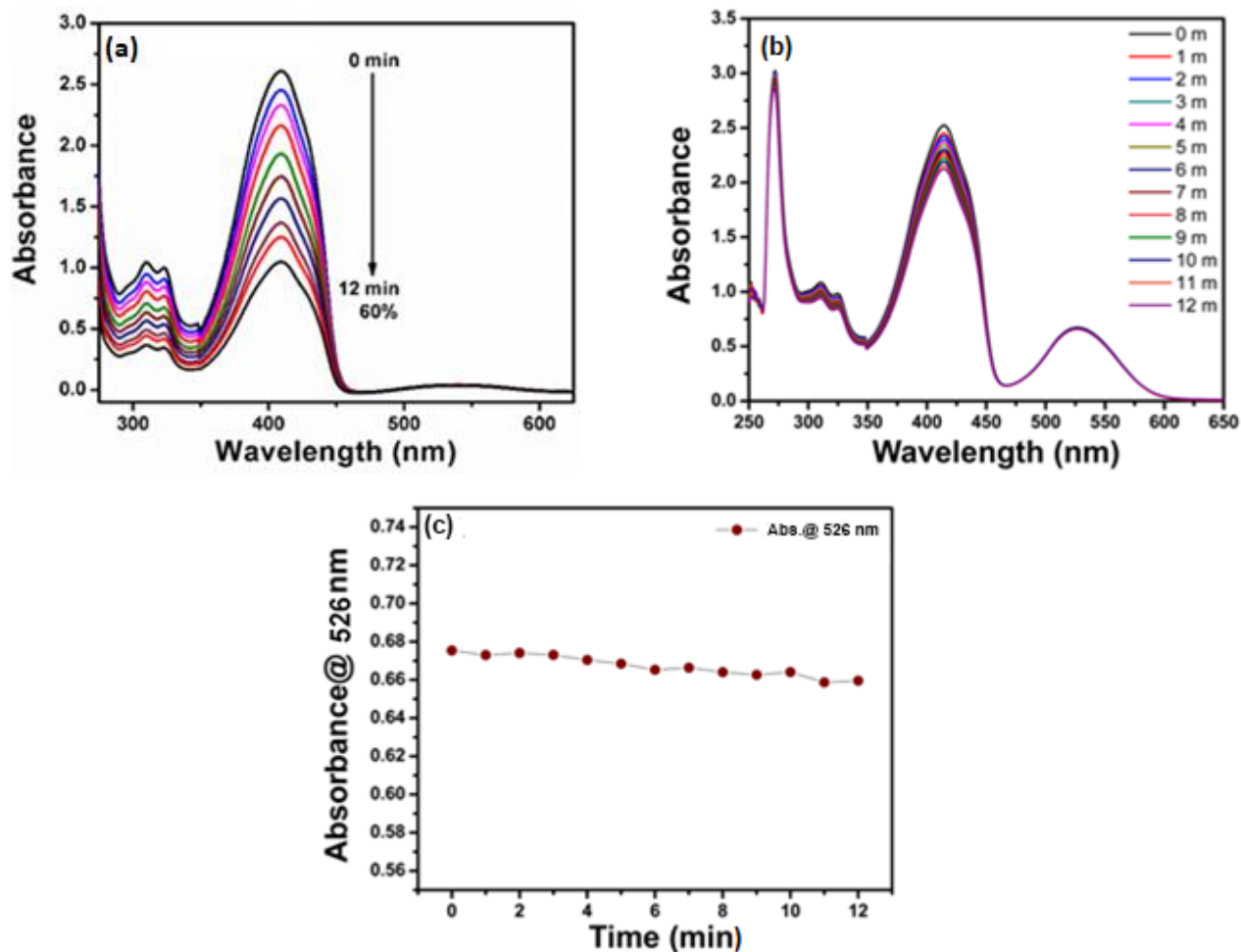
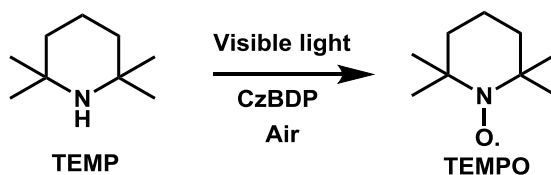


Fig. S18 Time-dependent absorption spectra of 1,3-diphenylisobenzofuran (DPBF): (a) in methanol (3 mL, 50 μ M) in the presence of CzBDP powder (1 mg), (b) in the presence of thermally annealed thin film of CzBDP upon irradiation with a green LED at 530 nm. (c) Photostability of the film under experimental conditions.

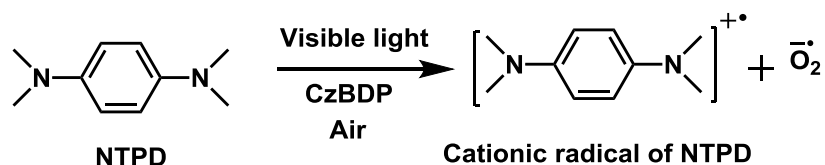
The generation of the singlet oxygen was also probed through the electron paramagnetic resonance (EPR) spectroscopy using 2,2,6,6-tetramethylpiperidine (TEMP) as a spin trapping agent. The characteristic EPR signals were observed due to the formation of TEMPO (oxidized form of TEMP) by singlet oxygen (Scheme S11, Main text Fig. 2b).²⁶



Scheme S11 Photochemical conversion of TEMP to TEMPO in the presence of singlet oxygen.

(c) Generation of superoxide anion radical

The generation of superoxide anion radical was monitored using O_2^- radical trapper *N, N, N', N'*-tetramethyl-*p*-phenylenediamine (NTPD) by UV-Vis experiment.²⁶ In a typical experimental procedure, 3 mL solution of NTPD in acetonitrile (200 mM) was taken in a cuvette and 1 mg of CzBDP polymer was added to it. The control experiment was carried out with the same amount and concentration of NTPD solution but without CzBDP. Both the solutions were stirred for 30 min under constant irradiation of visible light (9 W CFL) at room temperature. After 30 minutes, the resultant solutions were filtered by a syringe filter and transferred into two different cuvettes. A broad absorption in the region of 450 to 650 nm was observed for the solution with CzBDP (Fig. 2c, Main text). The broad spectrum is due to the formation of cationic radical of NTPD in the presence of O_2^- (Scheme S12).⁶ On the other hand, no characteristic absorption was observed for the solution without CzBDP revealing the capability of CzBDP for the generation of superoxide anion radical.



Scheme S12 Photochemical conversion of NTPD to cationic radical of NTPD in the presence of superoxide anion radical.

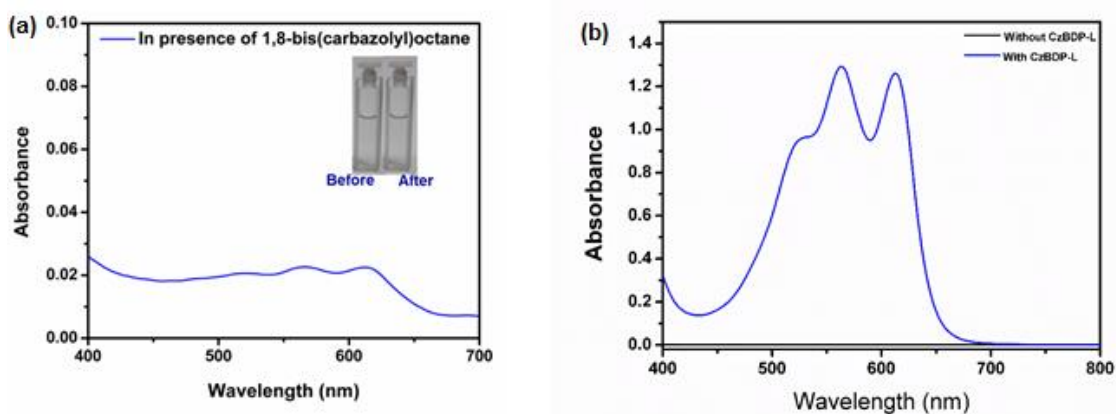
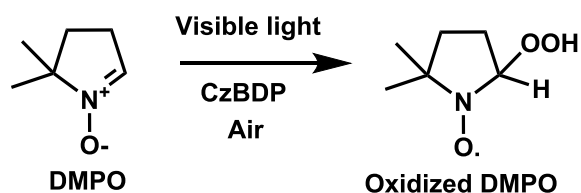


Fig. S19 Absorption spectra of *N, N, N', N'*-tetramethyl-*p*-phenylenediamine (NTPD) in acetonitrile (3 mL, 200 mM) in the presence of (a) 1,8-bis(carbazolyl)octane (1 mg) and (b) CzBDP-L (1 mg) upon irradiation by visible light (9W CFL, 30 min, with stirring).

The capability of superoxide anion radical generation by CzBDP was compared with alkylated carbazole and CzBDP-L under identical experimental conditions (3 mL, 200 mM NTPD in acetonitrile, 1 mg photosensitizer [1,8-bis(carbazolyl)octane/ CzBDP-L], irradiation by 9W CFL, 30 min, with stirring). No such visual color change was observed in the presence of 1,8-bis(carbazolyl)octane (Fig. S19a inset). UV-Vis experiment also revealed that the absorbance of the photoproduct is much lower than that of the solution containing CzBDP (Fig. S19a and Fig. 2c, Main Text). The soluble porous polymer (CzBDP) is more efficient ROS generator as compared to that of its linear counterpart as the optical density of NTPD cation radical generated by CZBDP is more than that of CzBDP-L (Fig. S19b and Fig. 2c, Main Text).

The generation of superoxide anion radical was also monitored via EPR experiment using 5,5-dimethyl-1-pyrroline-*N*-oxide (DMPO) which is well known for trapping the O_2^- . In the presence of superoxide anion radical, the EPR active oxidized product of DMPO was formed (Scheme S13, Fig. 2d, Main text).²⁶



Scheme S13 Photochemical conversion of DMPO to oxidized DMPO in the presence of superoxide anion radical.

VIII. Photooxidation of benzylamine

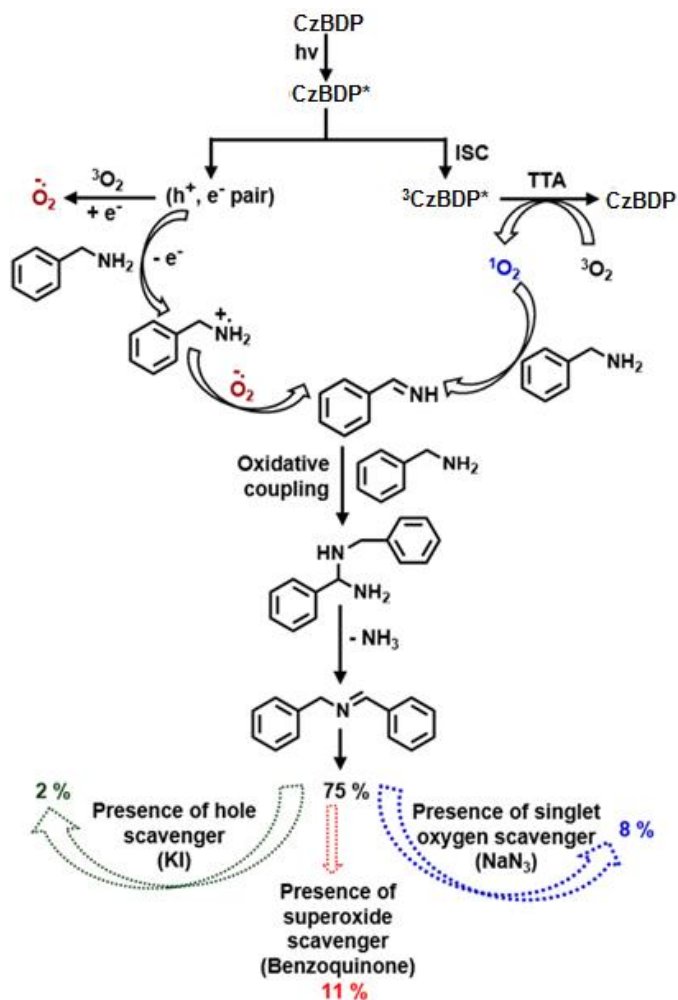
Photooxidation of benzylamine

Imines are important nitrogen-containing compounds having a vital role in different chemical and biochemical reactions. They are also very useful for the synthesis of fragrances, pharmacophores, industrial materials, bioactive molecules like nitrones, pyrrolines, chiral amines, oxaziridines, amides etc.^{27,28} Different strategies have been developed for the synthesis of imines, e.g, condensation of amines with carbonyl compounds, metal-catalyzed oxidation of primary or secondary amines and oxidative condensation of amines with alcohols. Nowadays, many metal-free catalysts were employed for the same purpose like azobisisobutyronitrile (AIBN), orthoiminoquinone, orthoquinone etc.²⁸ But often the high price and structural complexity are the bottlenecks for using of those catalysts. In this regard, the visible-light-driven photooxidation of amines is the alternative and effective way to overcome the related issues. Herein, the capability of CzBDP polymer for the generation of singlet oxygen and superoxide anion radical employed for the photooxidation of benzylamine as a model reaction.

Photooxidation of benzylamine was performed in a custom-made photoreactor using 9 W CFL bulb (Fig. S20). In a typical procedure, 1 mmol of benzylamine and ~1 wt.% of the polymer was taken in 3 mL acetonitrile and irradiated with 9 W CFL bulb under constant pressure of air (1 atm). The conversion of the reaction was monitored by ¹H NMR.

ROS mediated photooxidation of benzylamine can proceed through two distinct pathways. In the first case, the superoxide anion radical gets involved in the oxidation reaction whereas in another case the singlet oxygen. Based on the several control experiments, we propose that the photooxidation of benzylamine is happening due to the involvement of both the ROS (Scheme S14). The photoexcitation of CzBDP leads to the formation of exciton (electron and hole pair). Subsequently, molecular oxygen reduces to superoxide anion radical by accepting the photogenerated electron. Most likely, the oxidative coupling is regulated via the formation of cationic radical of benzylamine. In the next step, superoxide anion radical abstracts a proton and a hydrogen atom consequently to produce an imine intermediate. The by-product of the above reaction is H₂O₂ which was not detected due to the occurrence of similar cycles repetitively leading to the formation of imine and water (decomposition of H₂O₂).¹³ The photogenerated hole upon excitation of CzBDP can coordinate with nitrogen center of imine which makes the latter highly nucleophilic. Subsequently, a facile oxidative coupling reaction between imine and benzylamine gives the final product.¹⁴ On the other hand, the singlet oxygen assisted reaction is nearly similar to that of the mechanism of superoxide anion radical mediated reaction (Scheme S14). But the

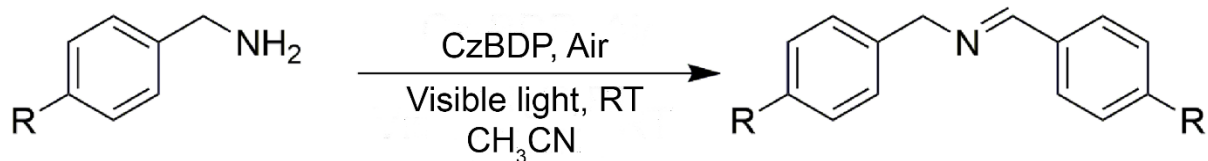
only difference, in this case, benzylamine directly reacts with singlet oxygen formed by photoexcitation of CzBDP to form the imine intermediate.²⁶



Scheme S14 The proposed reaction mechanism of ROS mediated photooxidation of benzylamine.

We found that the presence of CzBDP, air, and photoexcitation are essential for a significant conversion of benzylamine to the corresponding imine (Entry 1-4, Table S3). The controlled reactions were carried out in the presence of sodium azide (NaN_3) as a singlet oxygen scavenger, potassium iodide (KI) as a hole scavenger, and benzoquinone as a superoxide anion radical scavenger. It was found that the percentage of conversion decreased drastically for all these conditions (Entry 5-7, Table S3). These results illustrate that the photooxidation of benzylamine is controlled by CzBDP polymer through the generation of ROS (Scheme S14). The same coupling reactions were also carried out with the derivatives of benzylamine containing electron withdrawing (-F) and electron donating (- OCH_3) group in the para position (Entry 8,9 Table S3).²⁶

Table S3 Oxidative coupling of benzylamine using CzBDP, CzBDP thin film and CzBDP-L.



Entry	R	Reaction condition	Conversion
1	H	CzBDP, 15 h, hv	75%
2	H	Without CzBDP, 24 hv	2%
3	H	CzBDP, 24 h	3%
4.	H	CzBDP, 24 h, hv, argon	5%
5	H	CzBDP, 24 h, hv, NaN ₃	8%
6	H	CzBDP, 24 h, hv, KI	2%
7	H	CzBDP, 24 h, hv, benzoquinone	11%
8	F	CzBDP, 15 h, hv	61%
9	OMe	CzBDP, 15 h, hv	35%
10	H	Alkylated BODIPY, 24 h, hv	1%
11	H	1,8-bis(carbazolyl)octane, 24 h, hv	1%
12	H	CzBDP-L, 15 h, hv	30%
13	H	CzBDP thin film, 15 h, hv	35-40%

Entry 10 and 11 in Table S3 indicate that CzBDP is much more efficient for this oxidative coupling than that of the building units of the polymer. This is most probably due to the efficient ROS generation capability of CzBDP than that of the carbazole and BODIPY based building blocks. It was noticed that in presence of CzBDP-L, the percentage of conversion was decreased to 30% (Entry 12, Table S3), which is mostly due to the less efficient ROS generation capability of linear polymer (CzBDP-L) as compared to that of porous polymer (CzBDP). 40% conversion was observed in case of CzBDP thin film (Entry 13, Table S3).

All the photooxidation reactions were carried out in a custom-made photoreactor (Fig. S20) using 9 W CFL lamp as an excitation source under the constant stirring at 600 rpm. The % of conversion can be improved further by using suitable photoreactor ensuring homogeneous excitation of the reaction mixture under a continuous flow of air/ oxygen and increasing the power of the light source.

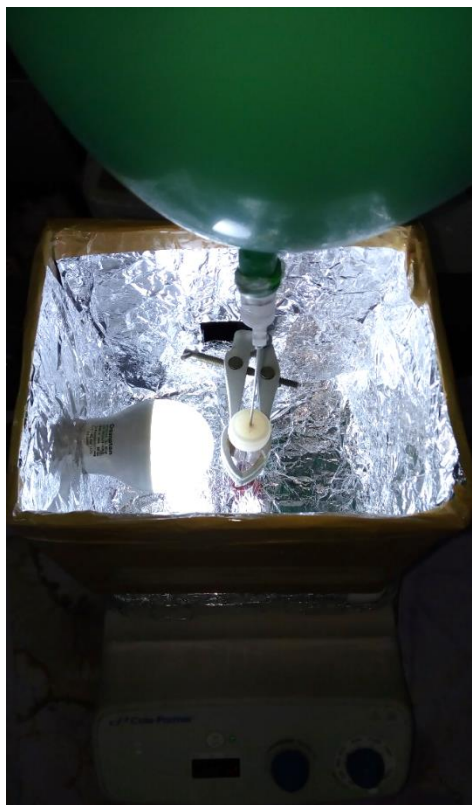


Fig. S20 Custom-made photoreactor utilized for the photooxidation reactions using 9 W CFL lamp as an excitation source with constant stirring at 600 rpm.

IX. Thin film fabrication and future scope

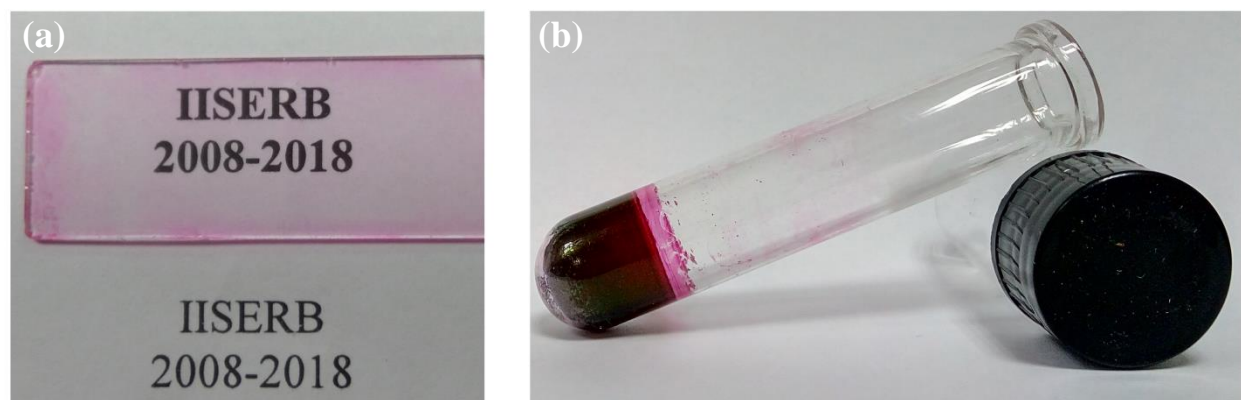


Fig. S21 (a) A transparent thin film of CzBDP polymer on quartz plate. (b) CzBDP thin film coated on the inner surface of the glass vessel used for photooxidation reaction.

The solution processability of CzBDP motivated us to prepare thin films. In a typical procedure, CzBDP was dissolved in dichloromethane and it was dip coated on a quartz plate. The fabricated thin film was observed to be highly stable. The thin film was heated at 60 °C for 10 minutes to obtain a thermally annealed homogeneous film with high degree of transparency (Fig. S21a). To check the capability of CzBDP thin film for the photooxidation reaction, CzBDP coated reaction vessel was prepared (Fig. S21b); the inner wall of the glass vessel was coated with CzBDP.

The advantage of thin film fabrication of CzBDP would broaden the scope of soluble CPOPs in the field of dip catalysts. The fabrication of large-scale photocatalytic devices based on soluble porous polymer would be possible using different techniques like 3D printing, roll-to-roll printing or inkjet printing in future.²⁹⁻³¹ On the other hand, the conjugated porous organic polymers are promising matrices for organic photovoltaics due to the efficient hole/ electron migration, enhanced phase separation and strong light absorption.³² Hence, the fluorescent thin film of porous polymers may serve as a new class of materials for organic electronics. Additionally, the efficacy of ROS generation will open up the new avenues for the soluble porous polymers as antimicrobial agents.

X. Comparative account of physicochemical properties of CzBDP with other notable porous materials

Table S4 Comparative account of physicochemical properties of CzBDP with other reported *soluble* porous organic polymers.

S.N.	System	S _{BET} (m ² g ⁻¹)	λ _{em} (nm) / (Φ)	ROS generation	Application	Reference
1.	CzBDP POP	180	610 / ~5 %	yes	Oxidation of benzylamine	<i>Present work</i>
2.	TIPS-CMP	12	---	---	Oxygen reduction reaction	<i>Angew. Chem. Int. Ed.</i> , 2017, 56 , 6946. ³³
3.	TPDC-BZ	610	580 / 46%	---	White light emission	<i>Chem. Commun.</i> , 2017, 53 , 1257. ³⁴
4.	HP2	514	643/ 12.9	---	Organic vapor detection	<i>Polym. Chem.</i> , 2016, 7 , 4213. ³⁵
5.	SHCPs	724	---	---	Gas storage and separation	<i>J. Mater. Chem. A</i> , 2016, 4 , 15072. ³⁶
6.	TPDC-DB	39	468 / 28%	---	Chemosensing	<i>Polym. Chem.</i> , 2015, 6 , 3775. ³⁷
7.	C-PIM	728	478 / NA	---	Gas adsorption	<i>Adv. Funct. Mater.</i> , 2014, 24 , 5219. ³⁸
8.	SCMP1	505	478 / NA	---	Gas adsorption	<i>Angew. Chem. Int. Ed.</i> , 2012, 51 , 12727. ³⁹

Table S5 Comparative account of ROS generation and ROS-induced photochemical reaction by CzBDP with notable porous materials based on porous organic polymers including those comprised of either carbazole (S. N. 2-8) or BODIPY-based monomers (S. N. 9-14), other POPs and covalent organic frameworks (S. N. 15-31), metal organic frameworks (S. N. 32-36) and linear conjugated soluble polymers (S. N. 37-38).

S. N.	System	S _{BET} (m ² g ⁻¹)	ROS generation				Photocatalysis reaction (Solution/ dispersion/ thin film)	Reference
			¹ O ₂		O ₂ ⁻			
			DPBF degradation	Trapping with TEMP	NTPD oxidation	Trapping with DMPO		
1	CzBDP POP	180	92%, 12 min, λ _{ex} = 530 nm	yes	Vis. light (9W CFL)	yes	Oxidation of benzylamine (in solution and thin film)	<i>Present work</i>
<i>POPs based on carbazole</i>								
2	C-CMP	---	NR	NR	150 W Xe lamp	NR	Oxidation of benzyl amine and thioanisole (dispersion)	<i>ACS Catal.</i> , 2016, 6 , 3594. ⁶
3	polyHIPE	230	NR	NR	NR	NR	Oxidation of thioanisole (dispersion)	<i>Chem. Commun.</i> , 2014, 50 , 8177. ⁴⁰
4	CzCP100, CzCP33	1077, 1280	NR	NR	NR (26 W CFL)	NR	Degradation of lignin β-O-4 models (dispersion)	<i>ACS Catal.</i> , 2017, 7 , 5062. ⁴¹
5	CF-HCP	1217	NR	yes	Green LED	yes	Oxidation of benzyl amine (dispersion)	<i>J. Mater. Chem. A</i> , 2017, 5 , 8697. ⁴²
6	CPOP-28, CPOP-29	NR	NR	yes	White LED	yes	Oxidation of sulfides, hydroxylation of arylboronic acids (dispersion)	<i>ACS Catal.</i> , 2018, 8 , 5313. ⁴³
7	Cz-POF-1	2065	NR	NR	NR	yes	α-Alkylation of aldehydes, oxidative	<i>ACS Catal.</i> , 2015, 5 , 2250. ⁴⁴

							hydroxylation of arylboronic acids, reductive dehalogenation of phenacyl bromide (dispersion)	
8	B-BT2-FL, B-BT-FL2	35-50	NR	NR	NR	NR	Photooxidation of α -terpinene (dispersion)	<i>Chem. Commun.</i> , 2013, 49 , 11158. ⁴⁵
<i>POPs based on BODIPY</i>								
9	BDT3	1010	NR	yes	NR	NR	Oxidation of thioanisole (dispersion)	<i>ACS Appl. Mater. Interfaces</i> , 2016, 8 , 27669. ³
10	CMP-BDP	299	NR	NR	NR	NR	Oxidation of thioanisole (dispersion)	<i>Macromolecules</i> , 2016, 49 , 1666. ⁴⁶
11	BDP-POP-1	358	5 min, green LED	NR	Low powered green LED	NR	NR	<i>Macromol. Chem. Phys.</i> , 2017, 218 , 1700101. ⁴⁷
12	BDP_CMP	769	NR	NR	NR	NR	α -terpinene into ascaridole (dispersion)	<i>Polym. Chem.</i> , 2016, 7 , 6662. ⁴⁸
13	CMPBDP-2	518	NR	NR	NR	NR	Oxidation of benzylamine (dispersion)	<i>J. Mater. Chem. A</i> , 2016, 4 , 17274. ⁴⁹
14	Iodic-BODIPY-PolyHIPE	230	NR	NR	NR	NR	Oxidation of thioanisole (dispersion)	<i>Chem. Asian J.</i> 2017, 12 , 392. ⁵⁰
<i>Other POPs and COFs</i>								
15	HOTT-HATN	526	NR	NR	NR (420 nm LED)	NR	Oxidation of benzylamine (dispersion)	<i>J. Mater. Chem. A</i> , 2017, 5 , 20180. ⁵¹

16	WCMP_0.4	244	NR	NR	NR (12W blue LED at 420 nm)	NR	Furoic acid into 5-hydroxy-2(5H)-furanone (dispersion)	<i>Chem. Commun.</i> , 2013, 49 , 2353. ⁵²
17	BF-CMP	1306	NR	NR	NR	NR	Degradation of rhodamin B (dispersion)	<i>Macromolecules</i> , 2018, 51 , 3443. ⁵³
18	B-BO-1,3,5	474	NR	yes	Blue LED	yes	Oxidation of benzylamine (dispersion)	<i>Adv. Mater.</i> , 2015, 27 , 6265. ²⁶
19	EY-POP-2	718	NR	NR	NR	NR	aza-Henry reaction (dispersion)	<i>RSC Adv.</i> , 2017, 7 , 408. ⁵⁴
20	MPC-CMPs	610	~ 99%, 30 min, $\lambda_{ex} =$ 700 nm	NR	-	-	NR	<i>Angew. Chem. Int. Ed.</i> , 2015, 54 , 6536. ²²
21	P4-1	162.4	NR	NR	NR	NR	Oxidation of benzylamine (dispersion)	<i>Polym. Chem.</i> , 2018, 9 , 1972. ⁵⁵
22	BDF-MON	455	NR	NR	Blue LED	NR	Oxidation of benzylamine (dispersion)	<i>Angew. Chem. Int. Ed.</i> , 2013, 52 , 6228. ⁵⁶
23	Bn-Anderson-CMP	218	NR	NR	NR	NR	Degradation of rhodamin B and methylene blue (dispersion)	<i>J. Mater. Chem. A</i> , 2017, 5 , 13757. ⁵⁷
24	FeP-CMP	1270	NR	NR	NR	NR	Oxidation of thioanisole (dispersion)	<i>J. Am. Chem. Soc.</i> , 2010, 132 , 9138. ⁵⁸
25	CMP_60	660	NR	NR	NR	NR	α -terpinene to ascaridole (dispersion)	<i>Angew. Chem. Int. Ed.</i> , 2013, 52 , 1432. ⁵⁹
26	Bead-BTZ,	NR	NR	NR	NR	NR	Oxidative hydroxylation of	<i>ACS Catal.</i> , 2017, 7 , 4602. ⁶⁰

	pHIPE-BTZ						arylboronic acids, (dispersion)	
27	B-BT	120	NR	NR	NR	yes	Regio-selective, stereo-selective [2 + 2] cycloaddition of styrene derivatives (dispersion)	<i>ACS Catal.</i> , 2017, 7 , 3097. ⁶¹
28	Polymer 1	198	NR	NR	NR	NR	Aza-Henry reactions, benzylamine oxidation (dispersion)	<i>ACS Catal.</i> , 2012, 2 , 417. ⁶²
29	MOP-1	586	NR	yes	Oxdn of DPD	yes	Photocatalytic bromination of 1, 2, 4-trimethoxy benzene (dispersion)	<i>ACS Catal.</i> , 2016, 6 , 1113. ⁶³
30	LZU-190	1035	-	-	20 W white LEDs	yes	Oxidative hydroxylation of arylboronic acids (dispersion)	<i>J. Am. Chem. Soc.</i> , 2018, 140 , 4623. ⁶⁴
31	COF-JLU5	1632	NR	yes	NR	yes	Photocatalytic C–C /C–P coupling reaction of N-phenyltetrahydro isoquinolines (dispersion)	<i>J. Mater. Chem. A</i> , 2017, 5 , 22933. ⁶⁵
<i>Metal organic frameworks (MOFs)</i>								
32	UNLPF-12	NR	NR	yes	14 W CFL	yes	Oxidation of benzyl amine, oxidative Mannich reactions (dispersion)	<i>ACS Catal.</i> , 2015, 5 , 5283. ⁶⁶
33	UNLPF-10	NR	NR	yes	NR	NR	Photo-oxygenation of sulfides (dispersion)	<i>J. Am. Chem. Soc.</i> , 2014, 136 , 15881. ⁶⁷
34	Sn ^{IV} (OH) ₂ TPyP	NR	NR	NR	NR	NR	Photo-oxygenation of sulfides, oxygenation of 1,5-dihydroxynaphthalene (dispersion)	<i>Inorg. Chem.</i> , 2011, 50 , 5318. ⁶⁸

35	Pt/PCN-224(Zn)	2018	NR	yes	Visible light, 100 mW/cm ²)	yes	Photooxidation of various aromatic alcohols (dispersion)	<i>J. Am. Chem. Soc.</i> , 2017, 139 , 2035. ⁶⁹
36	PCN-222	1659	NR	yes	NR	yes	Oxidative coupling of benzylamines (dispersion)	<i>Chem. Sci.</i> , 2018, 9 , 3152. ⁷⁰
<i>Soluble polymers</i>								
37	P-BODIPY-Silica	NR	DPA degradation	NR	NR	NR	Photooxidation of benzylamine (dispersion)	<i>Catal. Commun.</i> , 2015, 64 , 96. ⁷¹
38	WPF-Ir4, WPF-Ir8	NR	ADMA degradation	NR	NR	NR	NR	<i>Adv. Funct. Mater.</i> , 2014, 24 , 4823. ⁷²

#NR: not reported/ not mentioned

XI. ^1H , ^{13}C NMR spectra of all compounds

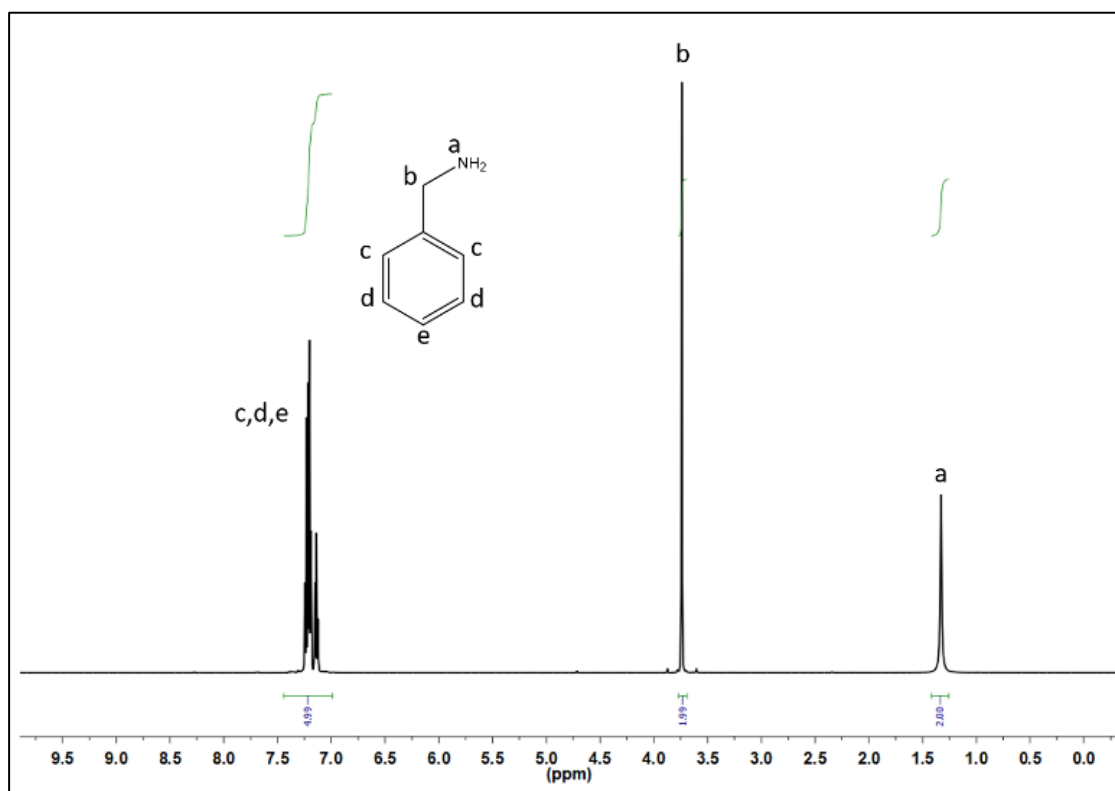


Fig. S22 ^1H NMR spectrum of benzylamine.

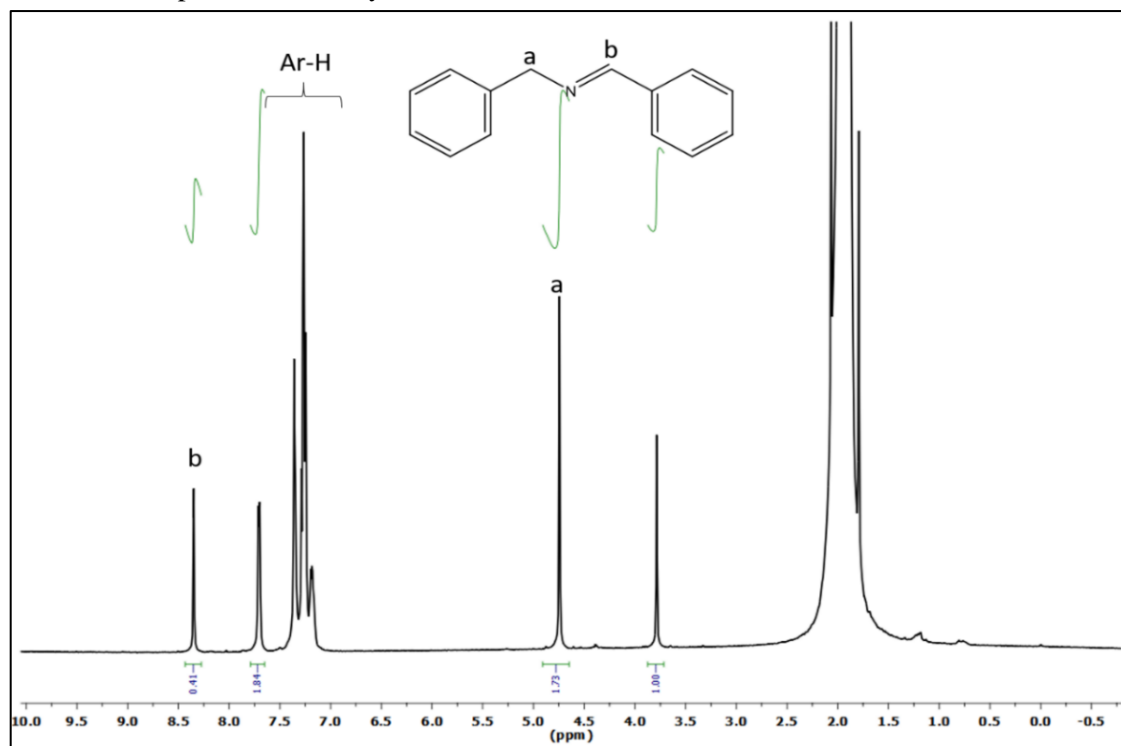


Fig. S23 ^1H NMR spectrum of the reaction mixture (Entry 1, Table S3).

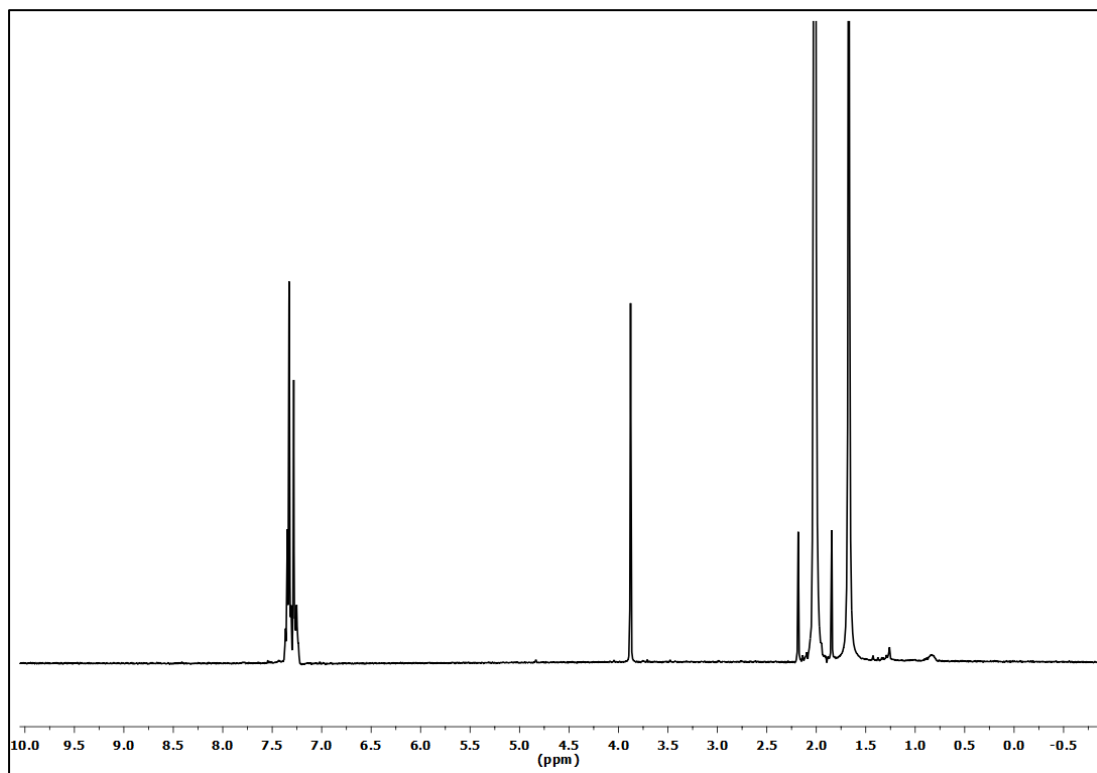


Fig. S24 ¹H NMR spectrum of the reaction mixture without catalyst (Entry 2, Table S3).

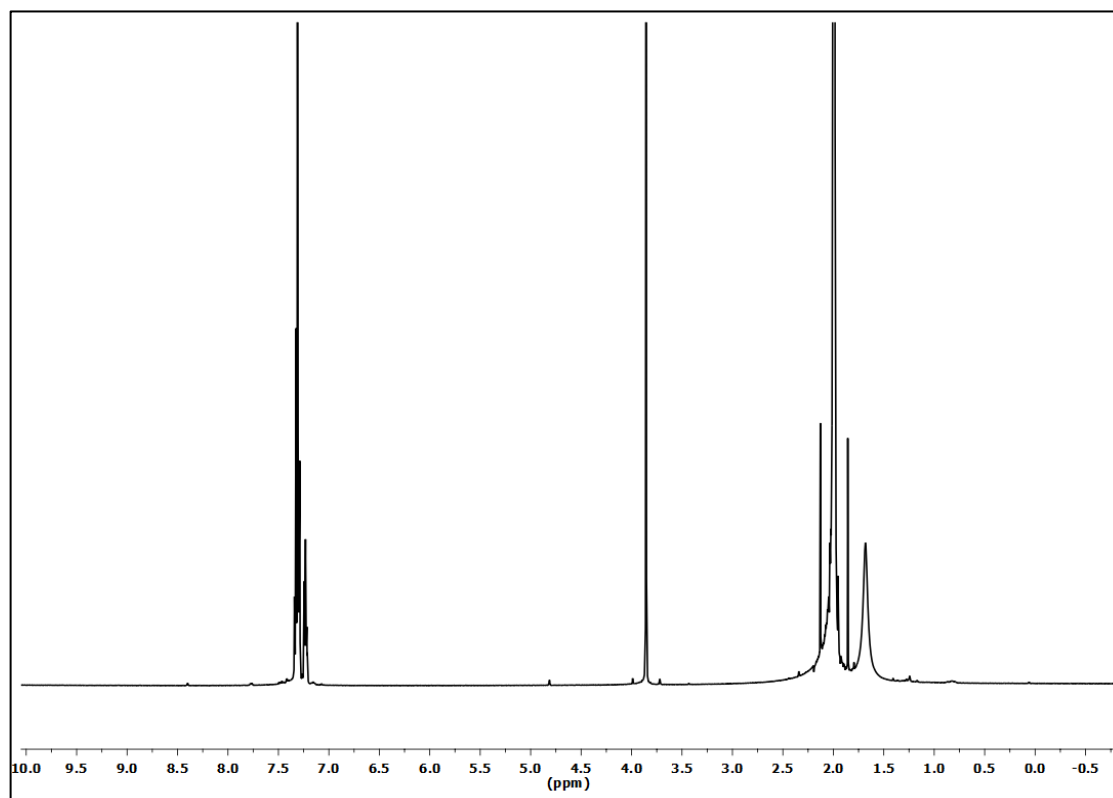


Fig. S25 ¹H NMR spectrum of the reaction mixture under dark (Entry 3, Table S3).

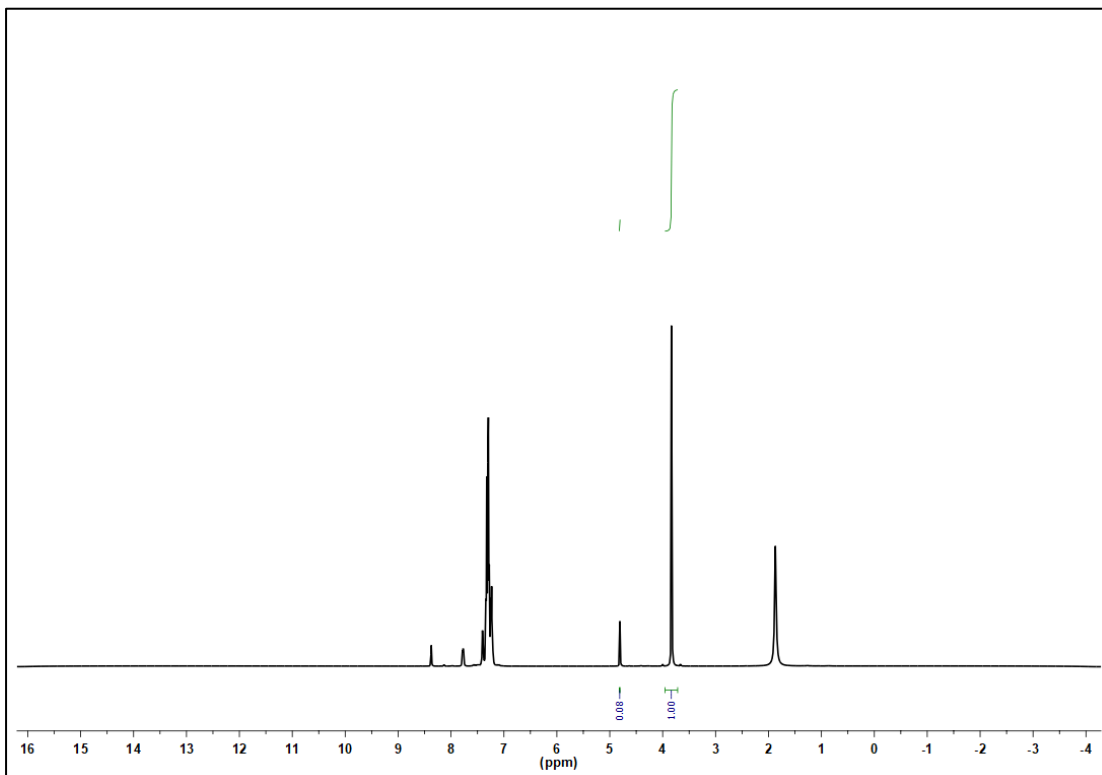


Fig. S26 ¹H NMR spectrum of the reaction mixture under argon atmosphere (Entry 4, Table S3).

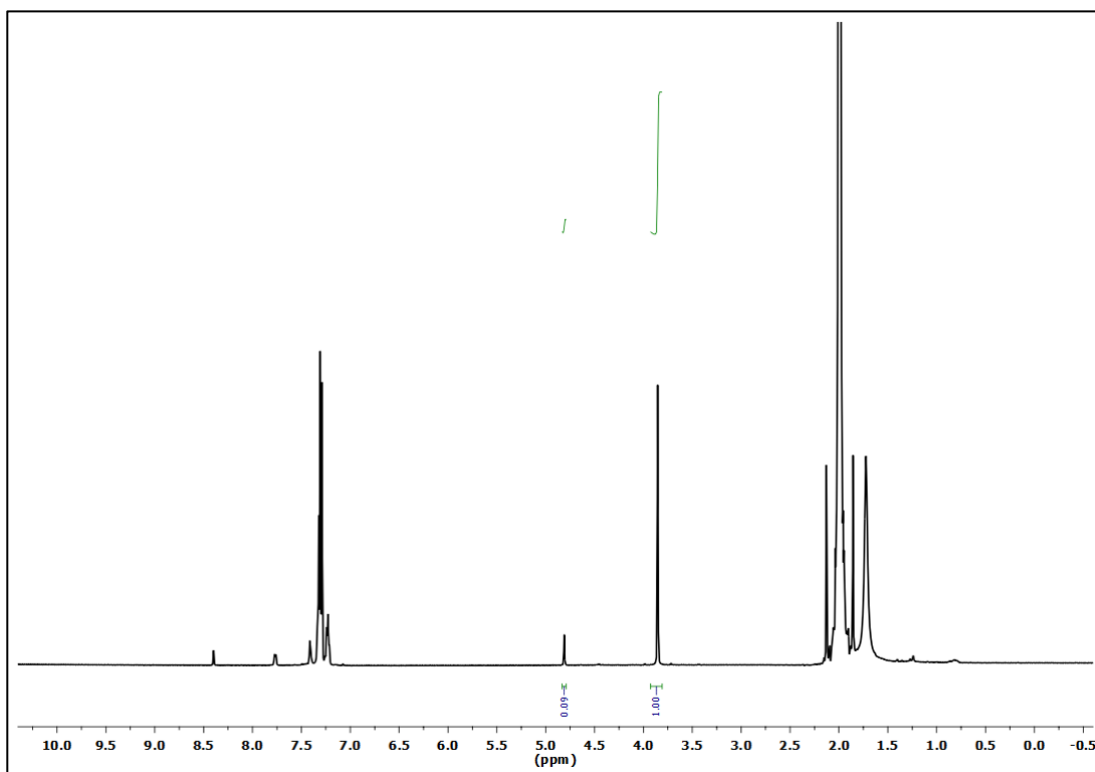


Fig. S27 ¹H NMR spectrum of the reaction mixture in presence of NaN₃ (Entry 5, Table S3).

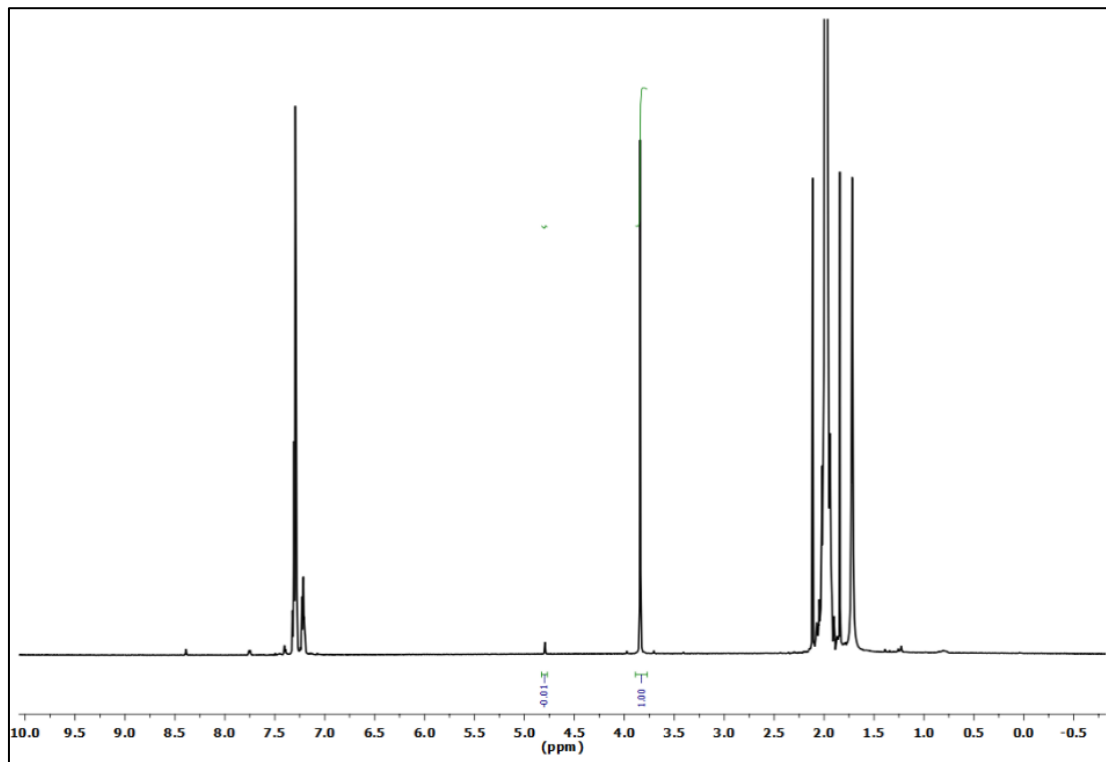


Fig. S28 ^1H NMR spectrum of the reaction mixture in presence of KI (Entry 6, Table S3).

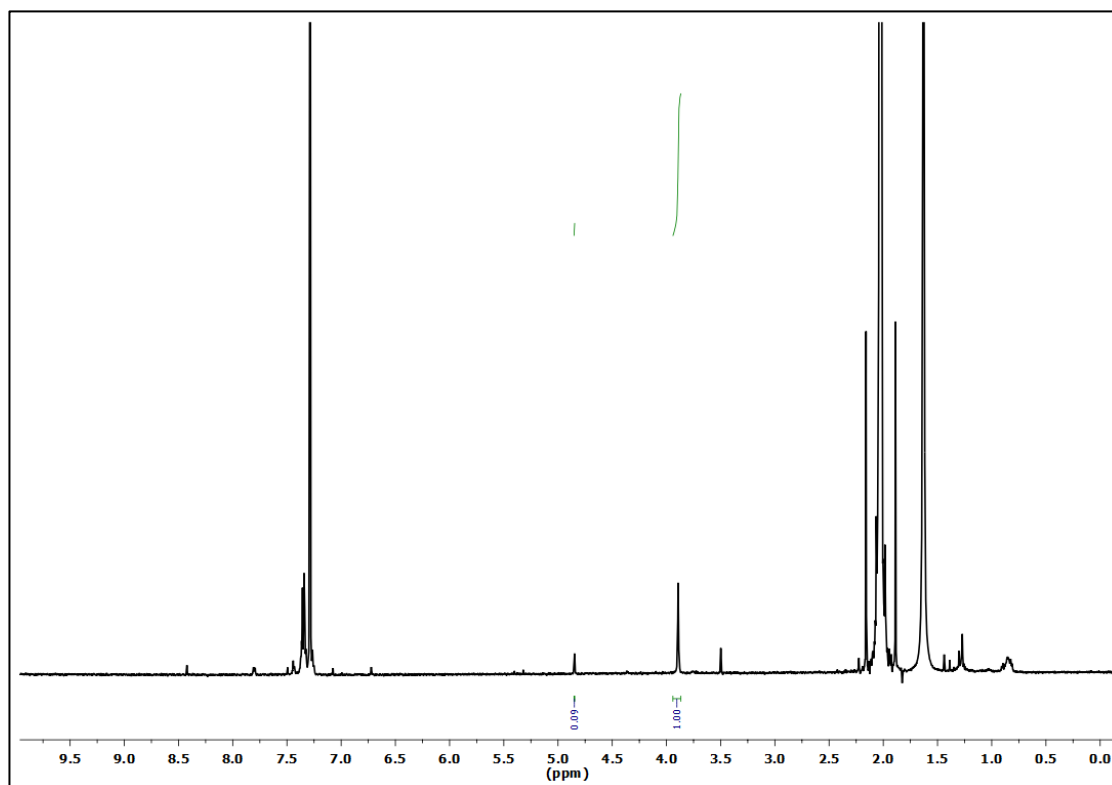


Fig. S29 ^1H NMR spectrum of the reaction mixture in presence of BQ (Entry 7, Table S3).

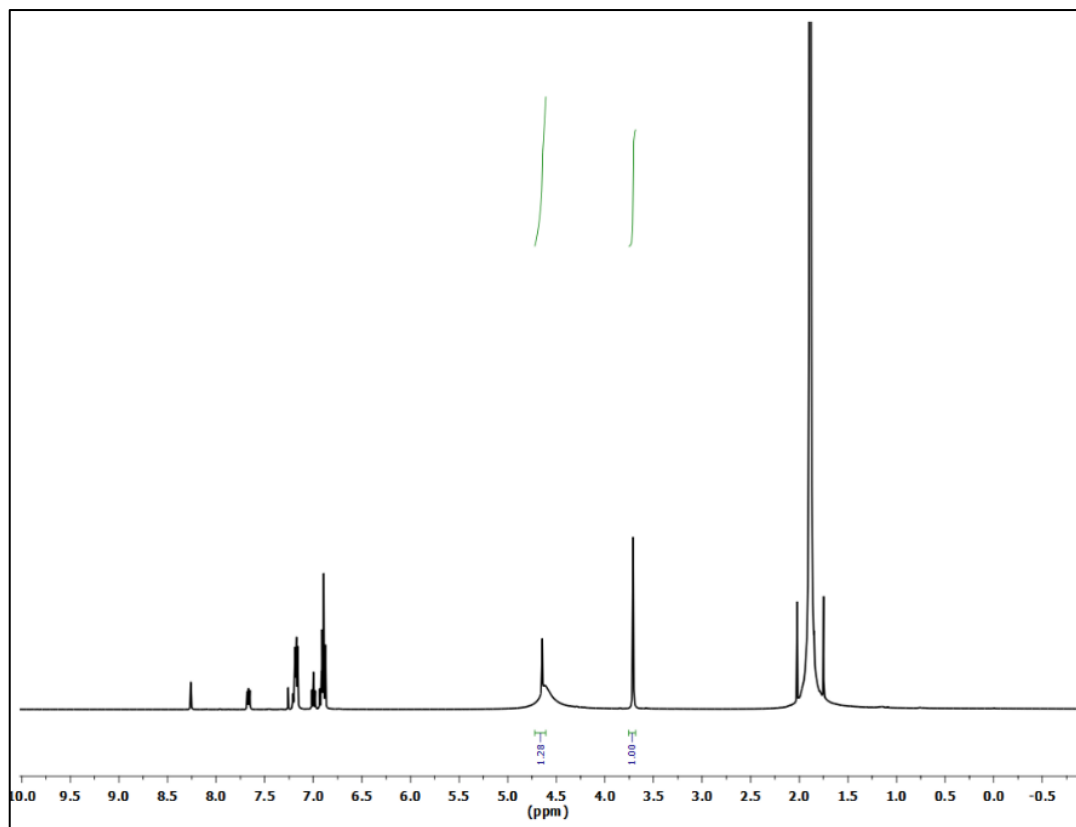


Fig. S30 ¹H NMR spectrum of the reaction mixture of (4-fluorophenyl)methanamine (Entry 8, Table S3).

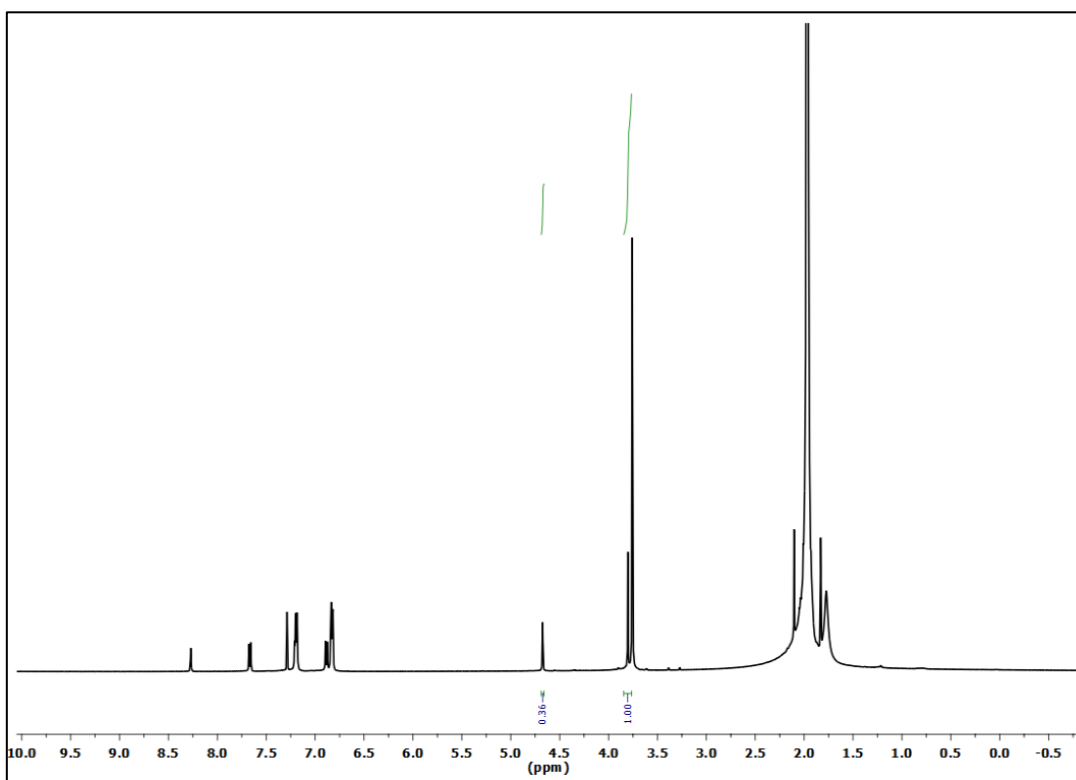


Fig. S31 ¹H NMR spectrum of the reaction mixture of 4-methoxybenzylamine (Entry 9, Table S3).

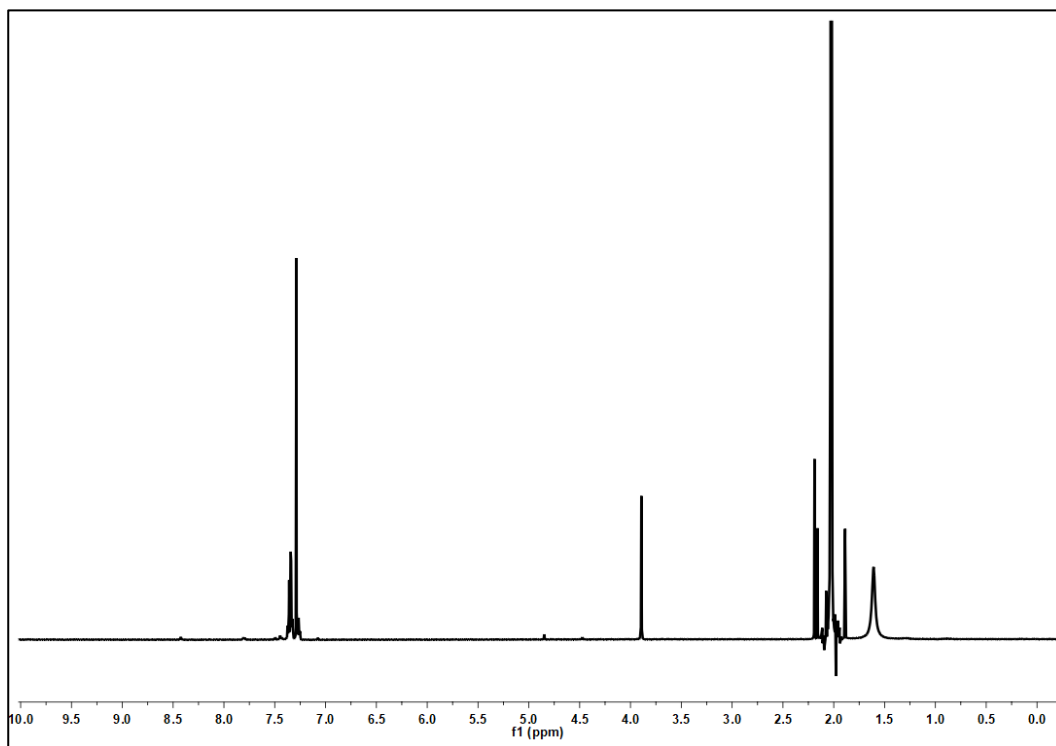


Fig. S32 ¹H NMR spectrum of the reaction mixture in presence of alkylated BODIPY (Entry 10, Table S3).

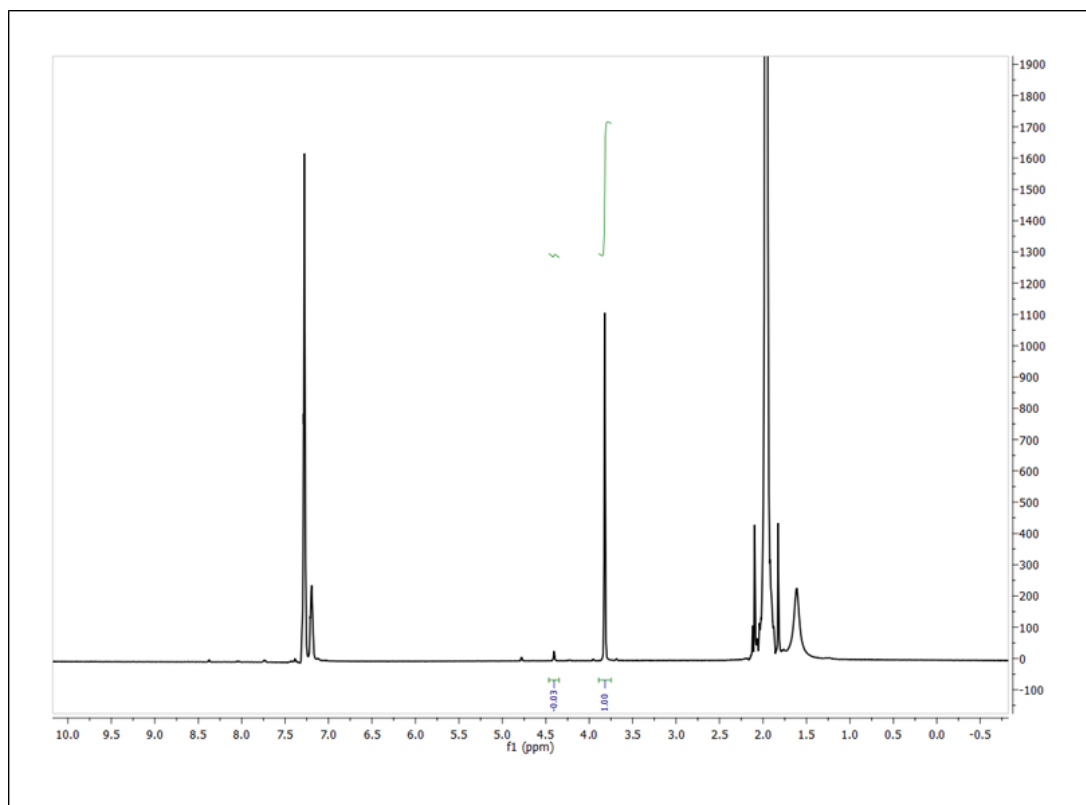


Fig. S33 ¹H NMR spectrum of the reaction mixture in presence of 1,8-bis(carbazolyl)octane (Entry 11, Table S3).

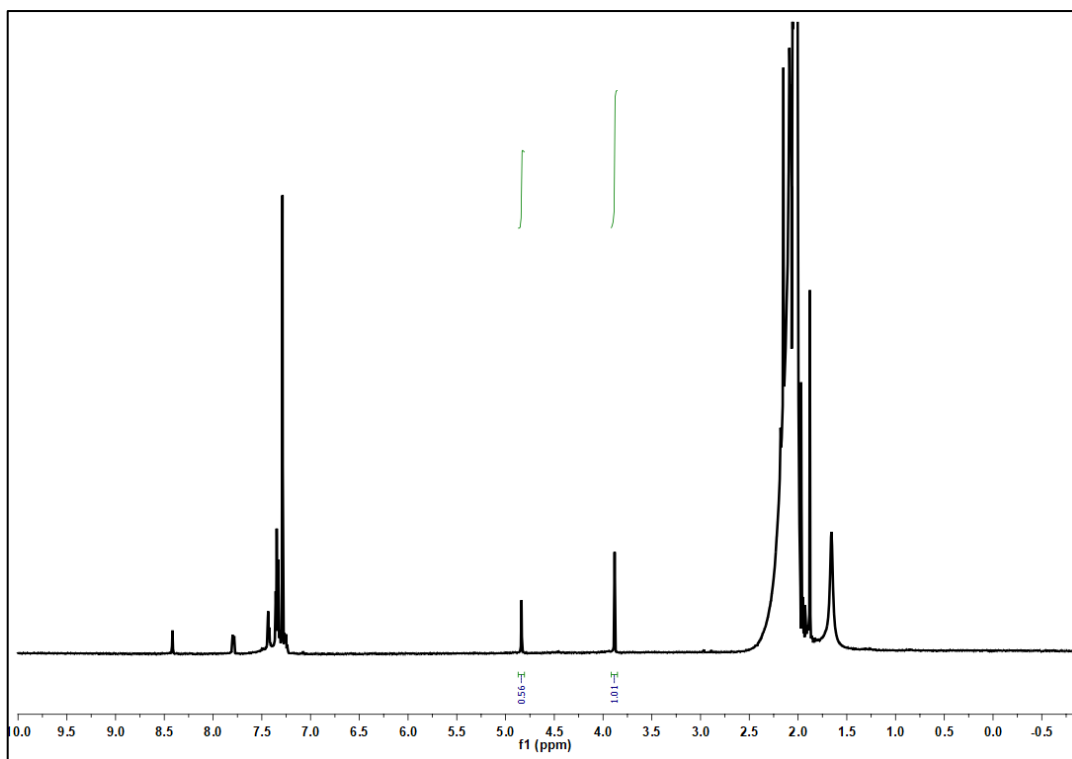


Fig. S34 ¹H NMR spectrum of the reaction mixture in presence of CzBDP thin film (Entry 13, Table S3).

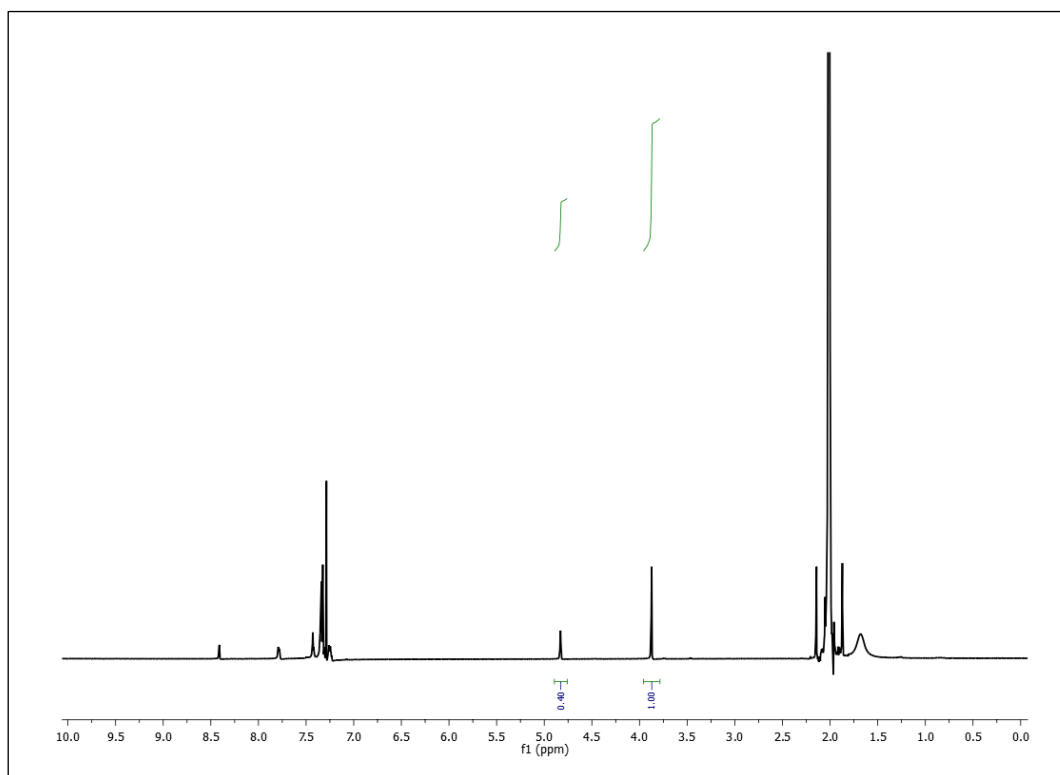


Fig. S35 ¹H NMR spectrum of the reaction mixture in presence of CzBDP-L (Entry 12, Table S3).

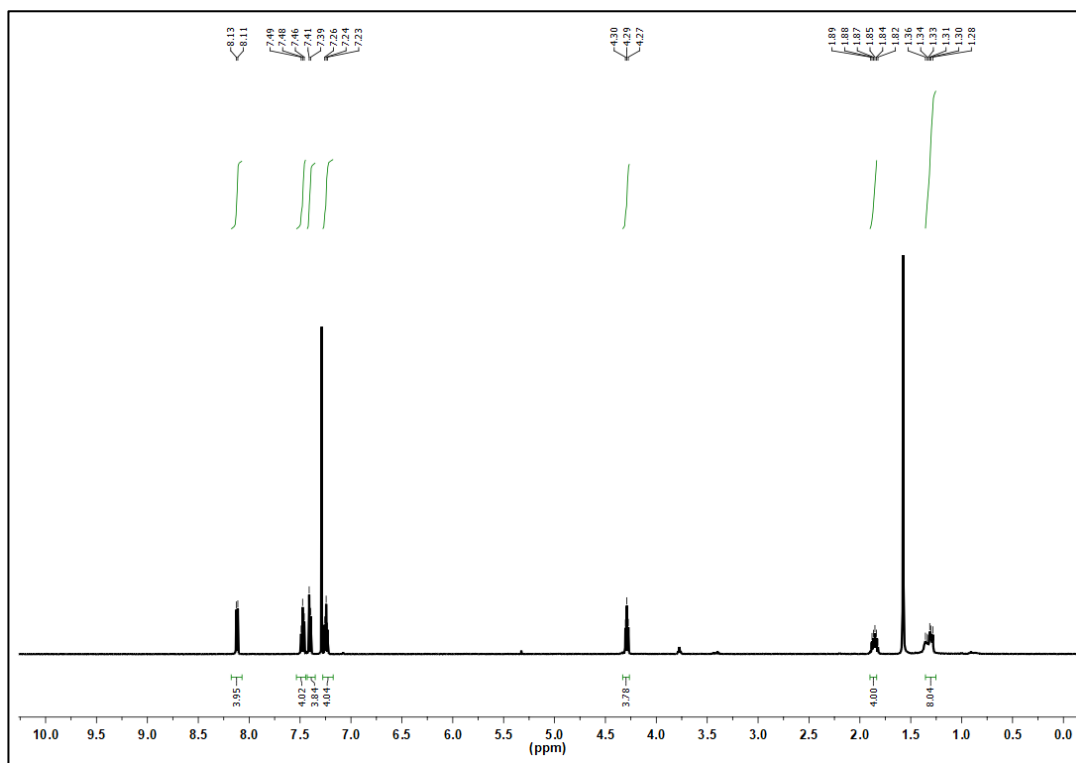


Fig. S36 ^1H NMR spectrum of 1,8-bis(carbazolyl)octane.

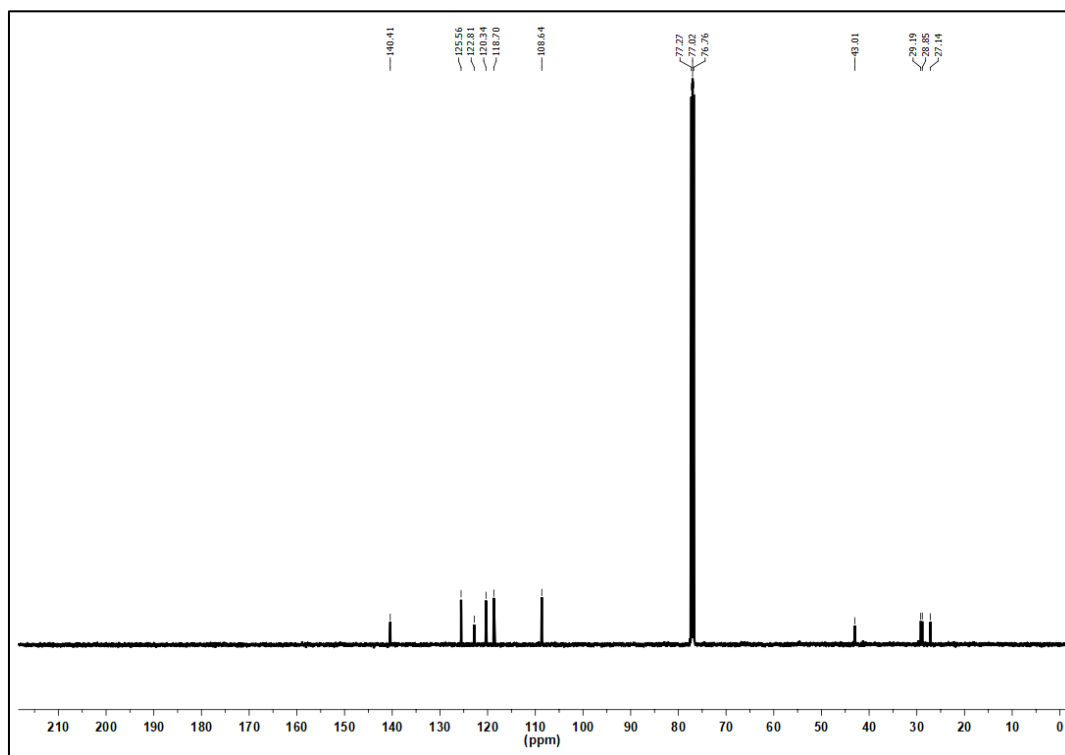


Fig. S37 ^{13}C NMR spectrum of 1,8-bis(carbazolyl)octane.

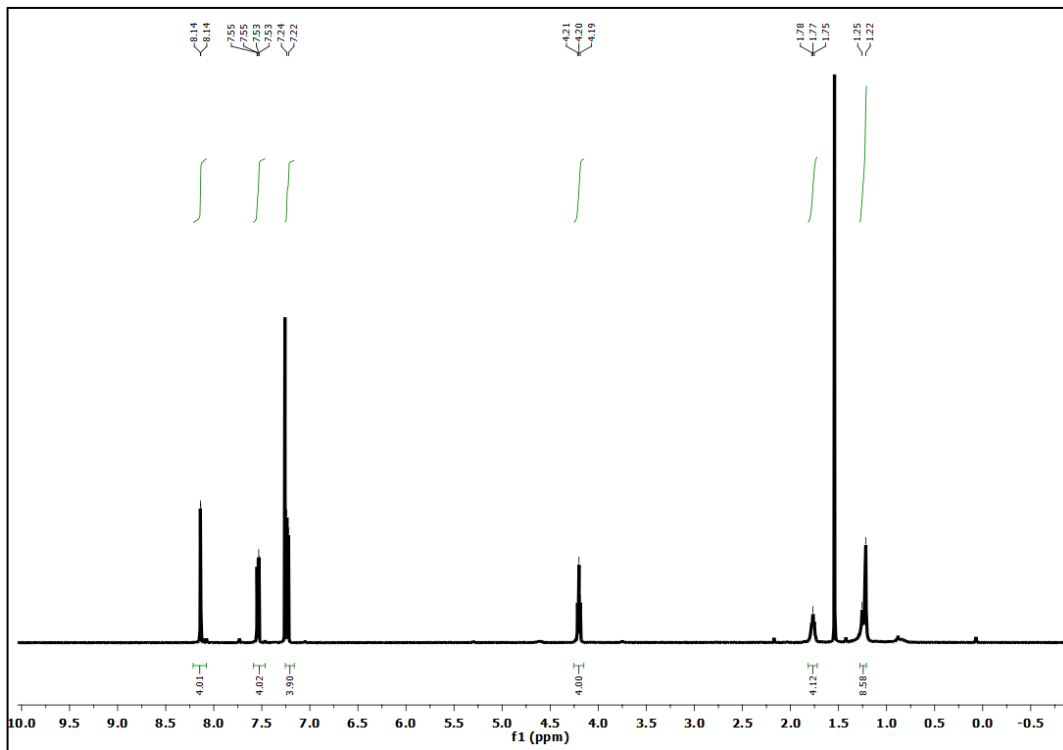


Fig. S38 ^1H NMR spectrum of 1,8-bis(3,6-dibromo-9H-carbazol-9-yl)octane.

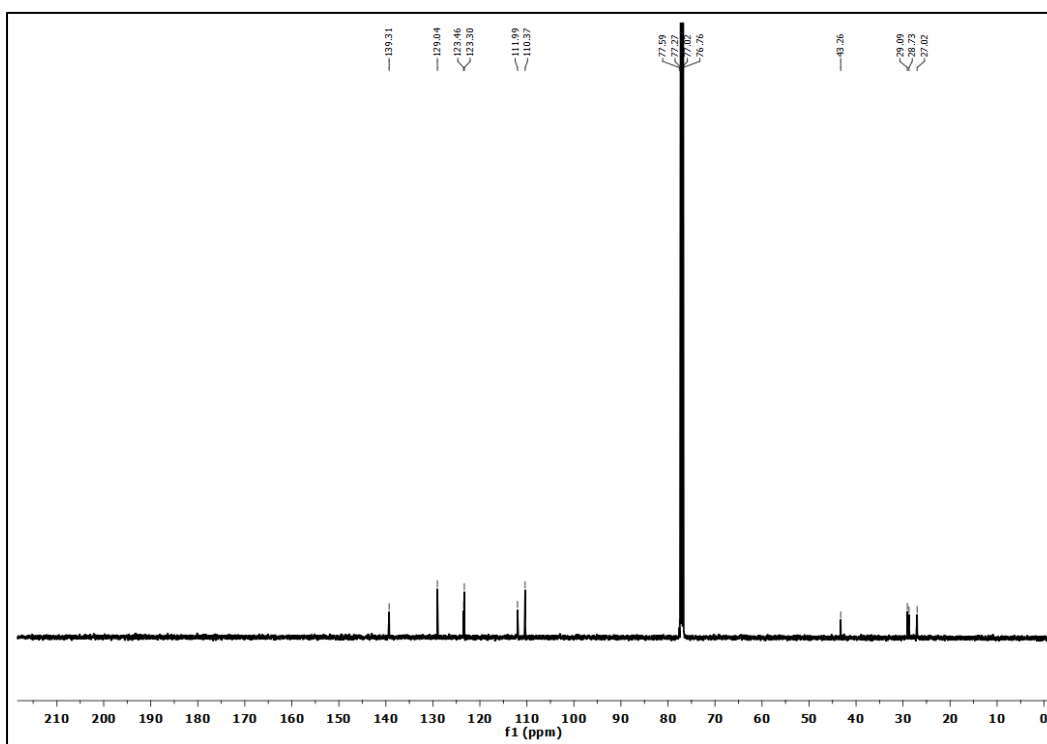


Fig. S39 ^{13}C NMR spectrum of 1,8-bis(3,6-dibromo-9H-carbazol-9-yl)octane.

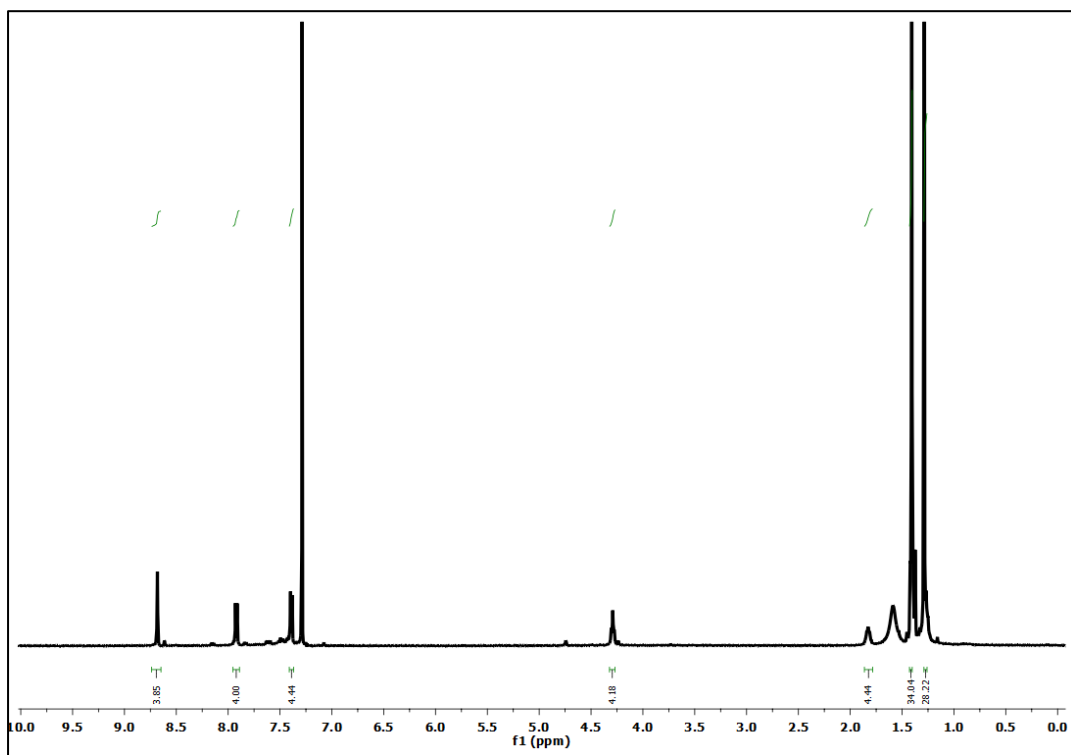


Fig. S40 ¹H NMR spectrum of 1,8-bis(3,6-bis(4,4,5,5-tetramethyl-1,3,2-dioxaborolan-2-yl)-9H-carbazol-9-yl)octane.

XII. References

1. E. Cloutet, C. Olivero, D. Adès, M. C. Castex and A. Siove, *Polymer*, 2002, **43**, 3489.
2. C. Gu, Y. Bao, W. Huang, D. Liu and R. Yang, *Macromol. Chem. Phys.*, 2016, **217**, 748.
3. S. Bandyopadhyay, A. G. Anil, A. James and A. Patra, *ACS Appl. Mater. Interfaces*, 2016, **8**, 27669.
4. X. Zhang, J. Lu and J. Zhang, *Chem. Mater.*, 2014, **26**, 4023.
5. Q. Chen and B. H. Han, *Macromol. Rapid Commun.*, 2018, **39**, 1800040.
6. C. L. Su, R. Tandiana, B. B. Tian, A. Sengupta, W. Tang, J. Su and K. P. Loh, *ACS Catal.*, 2016, **6**, 3594.
7. Y. Yuan, H. Huang, L. Chen and Y. Chen, *Macromolecules*, 2017, **50**, 4993.
8. M. Thommes, K. Kaneko, A. V. Neimark, J. P. Olivier, F. Rodriguez-Reinoso, J. Rouquerol, K. and S. W. Sing, *Pure Appl. Chem.*, 2015, **87**, 1051.
9. C. Würth, M. Grabolle, J. Pauli, M. Spieles and U. R. Genger, *Nat. Protoc.*, 2013, **8**, 1535.
10. Y. Nosaka and A. Y. Nosaka, *Chem. Rev.*, 2017, **117**, 11302.
11. Q. J. Hu, Y. C. Lu, C. X. Yang and X. P. Yan, *Chem. Commun.*, 2016, **52**, 5470.
12. C. Su, M. Acik, K. Takai, J. Lu, S. J. Hao, Y. Zheng, P. Wu, Q. Bao, T. Enoki, Y. J. Chabal and K. P. Loh, *Nat. Commun.*, 2012, **3**, 1298.
13. F. Su, S. C. Mathew, L. Möhlmann, M. Antonietti, X. Wang and S. Blechert, *Angew. Chem. Int. Ed.*, 2011, **50**, 657.
14. C. C. Winterbourn, *Nat. Chem. Biol.*, 2008, **4**, 278.
15. A. T. Y. Lau, Y. Wang and J. F. Chiu, *J. Cell. Biochem.*, 2008, **104**, 657.
16. (a) R. K. K. Mukherjee *Fundamental of Photochemistry* Wiley, New York, 1978; (b) J. R. Lakowicz, *Principles of Fluorescence Spectroscopy* Springer, New York, 2006.
17. M. S. Baptista, J. Cadet, P. D. Mascio, A. A. Ghogare, A. Greer, M. R. Hamblin, C. Lorente, S. C. Nunez, M. S. Ribeiro, A. H. Thomas, M. Vignoni and T. M. Yoshimura, *Photochem. Photobiol.*, 2017, **93**, 912.
18. P. Majumdar, R. Nomula and J. Zhao, *J. Mater. Chem. C*, 2014, **2**, 5982.
19. M. Hayyan, M. A. Hashim and I. M. AlNashef, *Chem. Rev.*, 2016, **116**, 3029.
20. T. L. Keevers and D. R. McCamey, *Phys. Rev. B*, 2016, **93**, 045210.
21. Y. Y. Cheng, T. Khoury, R. G. C. R. Clady, M. J. Y. Tayebjee, N. J. E. Daukes, M. J. Crossley and T. W. Schmidt, *Phys. Chem. Chem. Phys.*, 2010, **12**, 66.
22. X. Ding and B. H. Han, *Angew. Chem. Int. Ed.*, 2015, **54**, 6536.
23. M. Poß, H. Groger and C. Feldmann, *Chem. Commun.*, 2018, **54**, 1245.
24. S. A. Jenekhe and J. A. Osaheni, *Science*, 1994, **265**, 765.

25. K. Liu, Y. Liu, Y. Yao, H. Yuan, S. wang, Z. Wang and X. Zhang, *Angew. Chem. Int. Ed.*, 2013, **52**, 8285.
26. Z. J. Wang, S. Ghasimi, K. Landfester and K. A. I. Zhang, *Adv. Mater.*, 2015, **27**, 6265.
27. S. Furukawa, A. Suga and T. Komatsu, *Chem. Commun.*, 2014, **50**, 3277.
28. C. P. Dong, Y. Higashiura, K. Marui, S. Kumazawa, A. Nomoto, M. Ueshima and A. Ogawa, *ACS Omega*, 2016, **1**, 799.
29. M. M. Ling and Z. Bao, *Chem. Mater.*, 2004, **16**, 4824.
30. R. Søndergaard, M. Hösel, D. Angmo, T. T. L. Olsen and F. C. Krebs, *Mater. Today*, 2012, **15**, 36.
31. M. Ikawa, T. Yamada, H. Matsui, H. Minemawari, J. Y. Tsutsumi, Y. Horii, M. Chikamatsu, R. Azumi, R. Kumai and T. Hasegawa, *Nat. Commun.*, 2012, **3**, 1176.
32. H. Bildirir, V. G. Gregoriou, A. Avgeropoulos, U. Scherf and C. L. Chochos, *Mater. Horizons*, 2017, **4**, 546.
33. A. B. Marco, D. C. Lacalle, I. P. Miqueo, G. Valenti, A. Boni, J. Plas, K. Strutyński, S. D. Feyter, F. Paolucci, M. Montes, A. N. Khlobystov, M. M. Franco and A. M. Alonso, *Angew. Chem. Int. Ed.*, 2017, **56**, 6946.
34. P. Pallavi, S. Bandyopadhyay, J. Louis, A. Deshmukh and A. Patra, *Chem. Commun.*, 2017, **53**, 1257.
35. C. P. Sen, V. D. Goud, R. G. Shrestha, L. K. Shrestha, K. Arigab and S Valiyaveetil, *Polym. Chem.*, 2016, **7**, 4213.
36. Y. Yang, B. Tan and C. D. Wood, *J. Mater. Chem. A*, 2016, **4**, 15072.
37. S. Bandyopadhyay, P. Pallavi, A. G. Anil and A. Patra, *Polym. Chem.*, 2015, **6**, 3775.
38. G. Cheng , B. Bonillo , R. S. Sprick , D. J. Adams , T. Hasell and A. I. Cooper, *Adv. Funct. Mater.*, 2014, **24**, 5219.
39. G. Cheng, T. Hasell, A. Trewin, D. J. Adams and A. I. Cooper, *Angew. Chem. Int. Ed.*, 2012, **51**, 12727.
40. Z. J. Wang, S. Ghasimi, K. Landfester and K. A. I. Zhang, *Chem. Commun.*, 2014, **50**, 8177.
41. J. Luo, X. Zhang, J. Lu and J. Zhang, *ACS Catal.*, 2017, **7**, 5062.
42. Y. Zhi, Kun Li, H. Xia, M. Xue, Y. Mu and X. Liu, *J. Mater. Chem. A*, 2017, **5**, 8697.
43. H. P. Liang, Q. Chen and B. H. Han, *ACS Catal.*, 2018, **8**, 5313.
44. J. Luo, X. Zhang and J. Zhang, *ACS Catal.*, 2015, **5**, 2250.
45. K. Zhang, Z. Vobecka, K. Tauer, M. Antonietti and F. Vilela, *Chem. Commun.*, 2013, **49**, 11158.
46. M. Liras, M. Iglesias and F. Sánchez, *Macromolecules*, 2016, **49**, 1666.
47. D. G. Wang, Q. Li, Y. Zhu, H. Tang, M. Song and G.C. Kuang, *Macromol. Chem. Phys.*, 2017, **218**, 1700101.
48. J. M. Tobin, J. Liu, H. Hayes, M. Demleitner, D. Ellis, V. Arrighi, Z. Xu and F. Vilela, *Polym. Chem.*, 2016, **7**, 6662.

49. M. Liras, M. P. Sierra, M. Iglesias and F. Sa´nchez, *J. Mater. Chem. A*, 2016, **4**, 17274.
50. W. Li, L. Li, G. Cui, Y. Bai, X. Xiao, Y. Li and L. Yan, *Chem. Asian J.*, 2017, **12**, 392.
51. R. Xiao, J. M. Tobin, M. Zha, Y.L. Hou, J. He, F. Vilela and Z. Xu, *J. Mater. Chem. A*, 2017, **5**, 20180.
52. H. Urakami, K. Zhang and F. Vilela, *Chem. Commun.*, 2013, **49**, 2353.
53. B. Wang, Z. Xie, Y. Li, Z. Yang and L. Chen, *Macromolecules*, 2018, **51**, 3443.
54. C. A. Wang, Y.W. Li, X. L. Cheng, J. P. Zhang and Y. F. Han, *RSC Adv.*, 2017, **7**, 408.
55. H. Bohra, P. Li, C. Yang, Y. Zhao and M. Wang, *Polym. Chem.*, 2018, **9**, 1972.
56. N. Kang, J. H. Park, K. C. Ko, J. Chun, E. Kim, H. W. Shin, S. M. Lee, H. J. Kim, T. K. Ahn, J. Y. Lee and S. U. Son, *Angew. Chem. Int. Ed.*, 2013, **52**, 6228.
57. Y. Li, M. Liu and L. Chen, *J. Mater. Chem. A*, 2017, **5**, 13757.
58. L. Chen, Y. Yang and D. Jiang, *J. Am. Chem. Soc.*, 2010, **132**, 9138.
59. K. Zhang, D. Kopetzki, P. H. Seeberger, M. Antonietti and F. Vilela, *Angew. Chem. Int. Ed.*, 2013, **52**, 1432.
60. J. M. Tobin, T. J. D. McCabe, A. W. Prentice, S. Holzer, G. O. Lloyd, M. J. Paterson, V. Arrighi, P. A. G. Cormack and F. Vilela, *ACS Catal.*, 2017, **7**, 4602.
61. R. Li, B. C. Ma, W. Huang, L. Wang, D. Wang, H. Lu, K. Landfester and K. A. I. Zhang, *ACS Catal.*, 2017, **7**, 3097.
62. J. L. Wang, C. Wang, K. E. deKrafft and W. Lin, *ACS Catal.*, 2012, **2**, 417.
63. R. Li, Z. J. Wang, L. Wang, B. C. Ma, S. Ghasimi, H. Lu, K. Landfester and K. A. I. Zhang, *ACS Catal.*, 2016, **6**, 1113.
64. P. F. Wei, M. Z. Qi, Z. P. Wang, S. Y. Ding, W. Yu, Q. Liu, L. K. Wang, H. Z. Wang, W. K. An and W. Wang, *J. Am. Chem. Soc.*, 2018, **140**, 4623.
65. Y. Zhi, Z. Li, X. Feng, H. Xia, Y. Zhang, Z. Shi, Y. Mu and X. Liu, *J. Mater. Chem. A*, 2017, **5**, 22933.
66. J. A. Johnson, J. Luo, X. Zhang, Y. S. Chen, M. D. Morton, E. Echeverría, F. E. Torres and J. Zhang, *ACS Catal.*, 2015, **5**, 5283.
67. J. A. Johnson, X. Zhang, T. C. Reeson, Y. S. Chen and J. Zhang, *J. Am. Chem. Soc.*, 2014, **136**, 15881.
68. M. H. Xie, X. L. Yang, C. Zou and C. D. Wu, *Inorg. Chem.*, 2011, **50**, 5318.
69. Y. Z. Chen, Z. U. Wang, H. Wang, J. Lu, S. H. Yu and H. L. Jiang, *J. Am. Chem. Soc.*, 2017, **139**, 2035.
70. C. Xu, H. Liu, D. Li, J. H. Su and H. L. Jiang, *Chem. Sci.*, 2018, **9**, 3152.
71. Y. Zhou, Z. Zhou, Y. Li and W. Yang, *Catal. Commun.*, 2015, **64**, 96.
72. H. Shi, X. Ma, Q. Zhao, B. Liu, Q. Qu, Z. An, Y. Zhao, and W. Huang, *Adv. Funct. Mater.*, 2014, **24**, 4823.